Rowan University
Rowan Digital Works

Theses and Dissertations

9-23-2024

# INJECTABLE HYDROGELS THAT CAN MEASURE RADIATION AT BODY TEMPERATURE

Daniel Joseph Ball
*Rowan University*

Follow this and additional works at: https://rdw.rowan.edu/etd

 Part of the Biomedical Engineering and Bioengineering Commons, and the Chemical Engineering Commons

## Recommended Citation

Ball, Daniel Joseph, "INJECTABLE HYDROGELS THAT CAN MEASURE RADIATION AT BODY TEMPERATURE" (2024). *Theses and Dissertations*. 3296.
https://rdw.rowan.edu/etd/3296

This Thesis is brought to you for free and open access by Rowan Digital Works. It has been accepted for inclusion in Theses and Dissertations by an authorized administrator of Rowan Digital Works. For more information, please contact graduateresearch@rowan.edu.

# INJECTABLE HYDROGELS THAT CAN MEASURE RADIATION AT BODY TEMPERATURE

by

Daniel J. Ball

A Thesis

Submitted to the
Department of Biomedical Engineering
College of Engineering
In partial fulfillment of the requirement
For the degree of
Master of Science in Biomedical Engineering
at
Rowan University
April 26, 2024

Thesis Chair: Sebastián L. Vega, Ph.D., Professor, Department of Biomedical Engineering

Committee Members:
Erik Brewer, Ph.D., Professor, Department of Biomedical Engineering
Leonard Kim, D.A.B.R., Associate Professor of Radiation Oncology, Cooper Medical School of Rowan University

© 2024 Daniel J. Ball

## Dedications

To my parents Jim and Nancy Ball, my brother Jimmy, my sisters Ashley and Jessica, my niece Ella, and all other friends and family who have supported me during my time at Rowan University.

## Acknowledgments

I'm incredibly grateful to my research advisor Dr. Sebastián L. Vega for his support, encouragement, and mentorship. He provided me with the foundation for my research journey and equipped me with the skills necessary to evolve into the researcher I have become. Dr. Vega's guidance and mentorship have been invaluable, preparing me for the next phase of my life pursuits. I couldn't have imagined anyone else as my mentor during this time. Thank you to Dr. Vega and every member of the Vega lab who has contributed to my memorable experience.

I thank Dr. Kim, who, without his support, this research would not be possible. He has been a key collaborator from day one and has offered guidance and assistance to me whenever it was needed. I would also like to thank Dr. Brewer for his support. He was one of my favorite professors during my time at Rowan and has supported me even before my time as a Master's student.

I would also like to thank Cooper University Hospital, whose facilities played a large role in our data collection. Without resources available to me at Cooper University Hospital, I would not have had the necessary equipment required to complete my studies.

I thank Dr. Ibbott, whose guidance was very helpful in keeping this project in the right direction. These studies may have looked very different without your assistance.

Lastly, I'd like to thank my friends and family. Their support and kindness have been invaluable to me.

## Abstract

Daniel J. Ball
INJECTABLE HYDROGELS THAT CAN MEASURE RADIATION AT BODY TEMPERATURE
2022 - 2024
Advisor: Sebastián L. Vega, Ph.D.
Master of Science in Biomedical Engineering

Hydrogel-based radiation dosimeters are used to calibrate and validate radiation delivered by linear accelerators used in radiotherapy. Fricke hydrogel-based dosimeters with ferrous ion complexes oxidize when exposed to radiation, causing a measurable optical density change via a color shift in a photometric reagent. Gelatin-based Fricke hydrogels measure radiation but are unstable at body temperature, making noninvasive dose measurement inside a patient impossible. This study reports the synthesis and characterization of injectable hydrogels containing Fricke components that are stable at body temperature. The effects of varying individual Fricke hydrogel components on the sensitivity (measured by change in optical density) to radiation dose were systematically studied. Injectable dosimeter hydrogels were prepared using xylenol orange (XO) in the range of 0.05 to 0.5 mM, ferrous ammonium sulfate (Mohr's salt) in the range of 0.1 to 1 mM, and sulfuric acid in the range of 0 to 100 mM. The minimum concentration of Fricke components to create injectable dosimeter hydrogels that are sensitive to radiation dose (0 to 40 Gy) at room and body temperature was found to be XO (0.2 mM), sulfuric acid (25 mM) and Mohr's salt (0.5 mM). To assess biocompatibility, human mesenchymal stem cells (MSCs) were exposed to cylindrical Fricke-component hydrogels, and MSCs co-cultured with self-forming optimized hydrogels remained highly viable. Plans for a preclinical study using a rodent tumor model are underway, bringing this technology one step closer to clinical practice.

## Table of Contents

**Table of Contents (Continued)**

**Table of Contents (Continued)**

## List of Figures

## List of Tables

# Chapter 1

# Introduction

## 1.1 Cancer: Statistics and Treatment

Every year, there are more than 20 million new cases of cancer globally. Statistically, there are over 9 million fatalities resulting from the disease every year.[1] At the present time, common methods to treat cancer are as follows: chemotherapy, surgery, hormone therapy, immunotherapy, and radiation therapy.[2] Therapies used for blood cancers are chemotherapy, immunotherapy, radiation therapy, hormone therapy, and stem cell transplant therapy.[3,4] Therapies used for solid (tumor) cancers are mainly surgery, chemotherapy, and radiation therapy.[5,6] Chemotherapy is a drug treatment which utilizes powerful chemicals to kill fast growing, cancerous cells in the body. It is the most common treatment for cancer and is usually delivered in doses over a prescribed period. However, despite being the most common, chemotherapy has rather unpleasant side effects, including nausea, vomiting, diarrhea, hair loss, loss of appetite, fatigue, fever, mouth sores, pain, constipation, and easy bruising. It can also have some long lasting and irreversible side effects, including damage to lung tissue, heart problems, infertility, kidney problems, nerve damage (peripheral neuropathy), and the risk of cancer recurrence.[7] Chemotherapy can be used on its own to treat cancer depending on the circumstances. This is known as curative chemotherapy. Chemotherapy may also be used to make other forms of cancer treatment more effective. For instance, it can be applied to a patient before radiotherapy (chemoradiation) or used before surgery (neo-adjuvant chemotherapy). Alternatively, chemotherapy can be utilized to reduce the risk of cancer

returning after radiotherapy or surgery (adjuvant chemotherapy). If a cure is not possible, chemotherapy may be used to relieve cancer symptoms (palliative chemotherapy).[8,9]

Surgery is another commonly used method for treating cancer. In fact, it is one of the main treatments used providing that the circumstances for its use are met. This method involves the physical removal of hard, cancerous tumors and is generally very effective. It is most effective when the cancer is isolated to one area of the body. If the cancer can be entirely removed through the removal of tumorous tissue, this is the treatment that a patient would need. Generally, the earlier that the cancer is discovered, the easier it is to remove. Tumors that are removed with surgery are carcinomas, sarcomas, and melonomas.[10–12] Surgery can be performed as a sole curative measure for cancer. This is typically done when the cancer is found in one part of the body and it is likely that all of the cancer can be removed from the surgery alone.[13] It can also be performed before chemotherapy and radiotherapy as a means to make it easier for those treatments to attack a patient's cancer.[13,14] Sometimes, surgery is performed after chemotherapy and radiotherapy depending on the circumstances.[15] During surgery, the tumor itself along with some surrounding normal tissue is removed, which is known as the clear margin. Although surgery is efficacious at times, it is very invasive and painful to the patient receiving it, and it leads to complications including increased risk of infection post-treatment.[16,17]

Hormone therapy is a cancer treatment designed to slow or halt the growth of cancers that rely on hormones to develop. In doing so, this treatment also reduces the risk that the patient's cancer will return. Hormone therapy is most used for breast cancer, prostate cancer, and uterine cancer.[18] It is almost always used in conjunction with another

treatment. It can be a neoadjuvant treatment for surgery, radiation therapy, or chemotherapy. Hormone treatment can also be an adjuvant treatment as well.[19] The frequency at which this treatment is given depends on the type of cancer and the circumstances. For prostate cancer, a medicine is given to a patient monthly in the form of a shot that stops the patient from producing testosterone.[20] For breast cancer, patients can receive hormone therapy daily through a pill or monthly through a shot depending on the medicine they are given.[21] Due to this treatment interfering with a patient's ability to produce hormones or with how their hormones behave in their own body, it can cause undesirable side effects. The side effects generally depend on the patient's gender and the type of cancer that is being treated. They range from mood swings, breast size changes, hot flashes, diarrhea, nausea, and fatigue.[22]

Immunotherapy is a cancer treatment which helps prime a patient's immune system to fight cancer. This is an emerging and exciting technology. Originally discovered in the late 1800s by William Bradley Coley, this method of treatment wasn't widely recognized until 1967 when the existence of T-cells was discovered.[23] CAR T-cell therapy is mainly used clinically to treat blood cancers.[24] The most recent CAR T-cell therapy is for melanomas.[25] Now, immunotherapy is a quickly developing treatment that can effectively combat many types of cancer, including brain cancer, skin cancer, and breast cancer.[23,26] One type of immunotherapy available is T-cell transfer therapy, which boosts the natural ability of a patient's T-cells to fight cancer. This therapy works by taking immune cells directly from a patient's tumor, which are considered to be the most active against their cancer and then modifying T-cells in the lab so that they are able to recognize and combat the patient's cancer. These modified T-cells are then expanded *in*

*vitro* and then put back into the patient's body through an intravenous injection. However, a drawback to this methodology is that the patient's immune system, which has been enhanced to fight against cancer, also acts against healthy cells and tissues, causing undesirable side effects.[27] Another disadvantage to immunotherapy is that CAR T-cell therapy can cost upwards of $500,000, which is well out of the price range of most patients.[28]

Radiation therapy is another way to treat or manage the disease for many, though this depends on the specific circumstance of each patient's cancer. Some may even be able to go into remission with this treatment.[29] It works by using targeted radiation beams, which hit a cancerous tumor from multiple angles in order to destroy it. Radiation is often delivered through a linear accelerator (LINAC). These machines deliver high doses of radiation to shrink and kill cancer. At low doses, radiation can be used for X-rays to see inside a patient's body. At high doses, radiation can kill cancer cells and slow their growth, typically by damaging their DNA. When their genetic information is irreparably damaged, they are unable to divide, and as a result, cancer cells eventually die. These damaged cells are naturally removed from the body after dying. However, radiation therapy does not kill cancer cells right away. This process usually takes days or weeks to damage the DNA of cancer cells enough to kill them. Cancer cells will keep dying for weeks or months after treatment ends.[30–32] In terms of efficacy, non-invasiveness, and minimal side effects, radiation therapy may be the most desirable cancer treatment when available.

## 1.2 Radiation Therapy Treatment Process

After a cancer diagnosis, a CT (computed tomography) or MRI (magnetic resonance imaging) scan from the patient is obtained to create a 3D map of the tumor area and surrounding tissue. Following these scans, simulations can be performed. In this process, the scans are then used by a team of radiation oncologists to create an *in-silico* model for the treatment plan. The computer-based simulation of the radiation treatment plan predicts, with high accuracy, the radiation beam path from a LINAC to deliver adequate radiation dose to the tumor while minimizing the amount of radiation received by cancer-free adjacent tissues. This can be visualized via a 3D heat map, where darker colors generally represent areas that receive more radiation, and lighter colors generally represent areas that receive less radiation. Although these models are highly accurate, it is important to note that they are based on a computational simulation of a static CT or MRI scan, and actual results may vary due to patient movement which includes breathing, bowel filling, and passing gas.[33–35]

After this is done, the treatment plan can begin, and the patient can start receiving radiation. As previously mentioned, LINACs deliver radiation to the patient during these treatments, and they function by delivering external beams of radiation directly to the tumor through image guided radiation therapy and intensity modulated radiation therapy. Image guided radiation therapy (IGRT) is a method of cancer management that uses imaging technology to monitor the treatment throughout the entire process. Using adaptive radiation therapy (ART), an application of IGRT, doctors can adjust a patient's treatment plan mid-treatment to adapt to changes in the patient's anatomy and tumor size, allowing doctors to find the best approach for a given circumstance.[36]

Intensity modulated radiation therapy (IMRT) is a type of conformal radiation therapy. Conformal radiation therapy shapes the beams from a LINAC to closely fit the area of the cancer. LINACs have devices called multi-leaf collimators, which are made up of thin leaves of lead that can move independently while the LINAC moves around the patient. They can form shapes that fit precisely around the treatment area.[37] IGRT can guide IMRT, thus effectively combining the two therapies.[38] Beams of radiation from a LINAC eventually destroy the tumor over many treatments.[30,31] Radiation is delivered to a patient over multiple treatments because it would be dangerous to patient health to receive a full treatment dose all at once. Instead, radiotherapy is delivered in fractions over the course of several weeks. Fractions are small amounts of the total therapeutic dose required to treat a patient's cancer. A fraction is given to a patient on a scheduled day and repeated over the course of many days to add up to the total dose of radiation. Radiation is delivered in this manner because the patient receiving fractions of the total radiation dosage as opposed to the whole dose at once allows time for non-cancerous cells to repair themselves between treatments, reducing side effects.[39,40]

Radiation treatment dosages and fractions are quantified in centigray (cGy) and gray (Gy).[40] 1 Gy is equivalent to 1 Joule/Kilogram.[41] A linear accelerator measures its own radiation output using monitor units (MU), which are directly proportional to radiation dose. A LINAC is normally calibrated such that 1000 MU equals 10 Gy under a specific reference condition. Alternatively, radiation can be measured in monitor units (MU). A standard radiation treatment performed over the course of many weeks usually delivers 45-60 Gy to the patient.[42] As a reference, a person receives roughly 0.33 mSv from sun exposure every year on average.[43] Milliseverts (mSv) is another metric used to measure

radiation. 1 mSv represents the average accumulated background radiation that a person receives in a year from all sources in the United States, excluding radon. 1 mSv is the dose produced by exposure to 1 milligray (mG) or 0.001 Gy of radiation.[44] 0.33 mSv converts to 0.00033 Gy. This means that a patient receiving a 45 Gy radiation therapy treatment would receive roughly 150,000 years of sun exposure.

However, once the patient receives radiation treatment via LINAC, it is not possible to quantify the actual amount of radiation that the patient received and in what areas the radiation was received. This can cause radiation therapy to do more harm than benefit, over-irradiating patients and causing damage to surrounding tissues and undesired side effects.[45] It could also lead to under-irradiation, thus limiting the efficacy of radiation therapy in treating the cancer. Ultimately, if the cancer is not fully treated due to a lack of dosimetric verification, then the cancer could potentially come back and the process of treating cancer through radiation therapy could become a cycle. In summary, either a target area can receive too much radiation from the treatment, causing unnecessary damage to surrounding tissue, or the target area can receive too little radiation, potentially leading to a resurgence of the cancer and more radiation treatments than necessary.[46,47] An implantable dosimeter that can verify radiation delivered to the body in 3D and real time would address the current limitations of radiation therapy.

### 1.3 Radiation Dosimetry

Radiation dosimetry is used to measure and quantify radiation. There are several methods for dosimetric verification, all with their own advantages and disadvantages. A dosimeter is an instrument used for measuring and monitoring exposure to radiation, such as X-rays and gamma rays.[48] Traditionally, they are small devices that can be worn on the

body to monitor the personal accumulated radiation dose received by an individual from external sources.[49] In modern times, dosimeters come in a variety of forms. Three common dosimeters are Geiger counters, radiochromic films, and dosimeter hydrogels.[50,51]

One of the most common and easy to use dosimetric verification devices is the Geiger counter. A Geiger counter is a device that is frequently used as a safety measure for doctors who deliver radiation to patients. Geiger counters work through the principle of ionization, a process in which atoms gain or lose electrons and become electrically charged. The greater the amount of ionization, the greater the amount of radiation that there is at a particular point.[52] A significant limitation of Geiger counters is that they can only measure radiation at a single point in space (1D). Additionally, Geiger counters cannot be implanted in a patient and can only detect radiation that is present at the moment. Once the LINAC is switched off, the radiation stops, and since patients are not radioactive after treatment, there is nothing for the device to detect. Overall Geiger counters are a poor dosimeter to use for dosage verification on a cancer radiation therapy patient.

Another commonly used dosimeter is a radiochromic film. These are two dimensional films that provide dose measurements at high resolution. These films work through modification of structural characteristics of their crystalline sensitive elements when exposed to ionizing radiation.[53] However, radiochromic films are limited in the sense that they cannot be implanted and they only measure radiation in two dimensions. This means that no depth dependence of radiation can be assessed. Overall, radiochromic films are not ideal for dosage verification on cancer radiation therapy patients.

Hydrogel dosimetry is a tool that can be used to provide dosimetric measurements at high accuracy and in three dimensions (3D). The "Fricke gel" dosimeter utilizes the oxidation of ferrous ions into ferric ions upon exposure to radiation to function.[54,55] At present, these hydrogels are primarily used for LINAC calibration. For the purposes of resolution-time-accuracy-precision (RTAP), a three-dimensional dosimeter must be able to deliver a 3D dosimetric analysis of a treatment plan with 1 mm isotropic spatial resolution, within 1 hour, with an accuracy of within 3% of the true value, with 1% precision. Dosimeter hydrogels are the only dosimeters that have acceptable RTAP. Therefore, by this metric, dosimeter hydrogels are the only true 3D dosimeters available for radiotherapy calibrations.[56] For this reason, some believe that dosimeter hydrogels are the best available option for dosage verification on cancer radiation therapy patients.

### 1.4 Fricke Hydrogel Dosimeters

As discussed in the preceding section, hydrogel dosimetry is a tool that can be used to calibrate linear accelerators used in the treatment of cancer patients. One of the earliest hydrogel dosimeters is known as "Fricke gel," which utilizes gelatin as its primary base. These hydrogels were inspired by the work Hugo Fricke and Sterne Morse in 1927, the former being whom the hydrogels were named after. Their studies later led to the use of nuclear magnetic resonance (NMR) to measure radiation-induced chemical changes while stabilizing the dose information via a gelatin matrix in the 1980s. While these hydrogels were originally simple in nature, many commonly used "Fricke components" or dosimeter components were later added to the hydrogel, creating what is now modern-day hydrogel dosimetry.[57]

These hydrogels generally utilize Ferrous ions ($Fe^{2+}$) in the form of Mohr's Salt, which turn into Ferric ions ($Fe^{3+}$) when irradiated, and sulfuric acid, which is used to control the gel sensitivity. When a Fricke dosimeter hydrogel containing Xylenol Orange is irradiated, it goes from a light orange color to a darker orange corresponding to the amount of radiation that the hydrogel receives (Figure 1). Many studies have worked with optical CT scanners or various spectrometry technologies to characterize various versions of Fricke dosimeter hydrogels, and it is generally found that their peak absorbance light wavelengths are 435 nm when they are unirradiated and 585 nm when they are irradiated.[54,56,58–70]

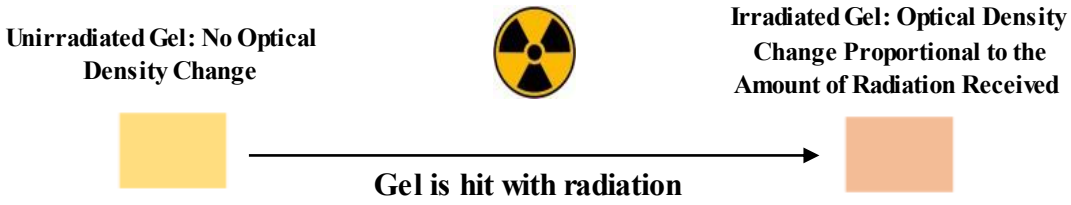


*Figure 1*. Dosimeter Hydrogel Response to Radiation. A representation of the physical change that Fricke xylenol orange dosimeter hydrogels undergo in exposure to radiation. As hydrogels absorb radiation, they go from a light orange color to a darker orange proportional to the amount of radiation they receive.

When a beam of radiation hits the hydrogel, it creates free radicals out of the water within the now solid solution. Free radicals have at least one unpaired electron in

their outer shell, making them highly reactive. This state allows a free radical to oxidize nearby ions. In this case, it oxidizes ferrous ions. This interaction is the entire basis in which Fricke hydrogel dosimetry functions. However, we cannot optically measure the change of ferrous to ferric ions without a visual agent such as xylenol orange. When ferrous ions become ferric ions, they bind to structures of xylenol orange. It is important to note that ferrous ions cannot bind to xylenol orange structures. When ferric ions bind to structures of xylenol orange, it results in a chemical change that causes the structures to go from a light orange color (435 nm) to a dark orange color (585 nm) (Figure 2). However, free radicals will form on their own in an aqueous solution without exposure to radiation. As a counter measure to this, sulfuric acid is commonly used as an antioxidant, keeping ferrous ions stable until the hydrogel is exposed to radiation. This raises the sensitivity of the dosimeter as it will lower the chance of false photometric readings.[54,56,58–70]

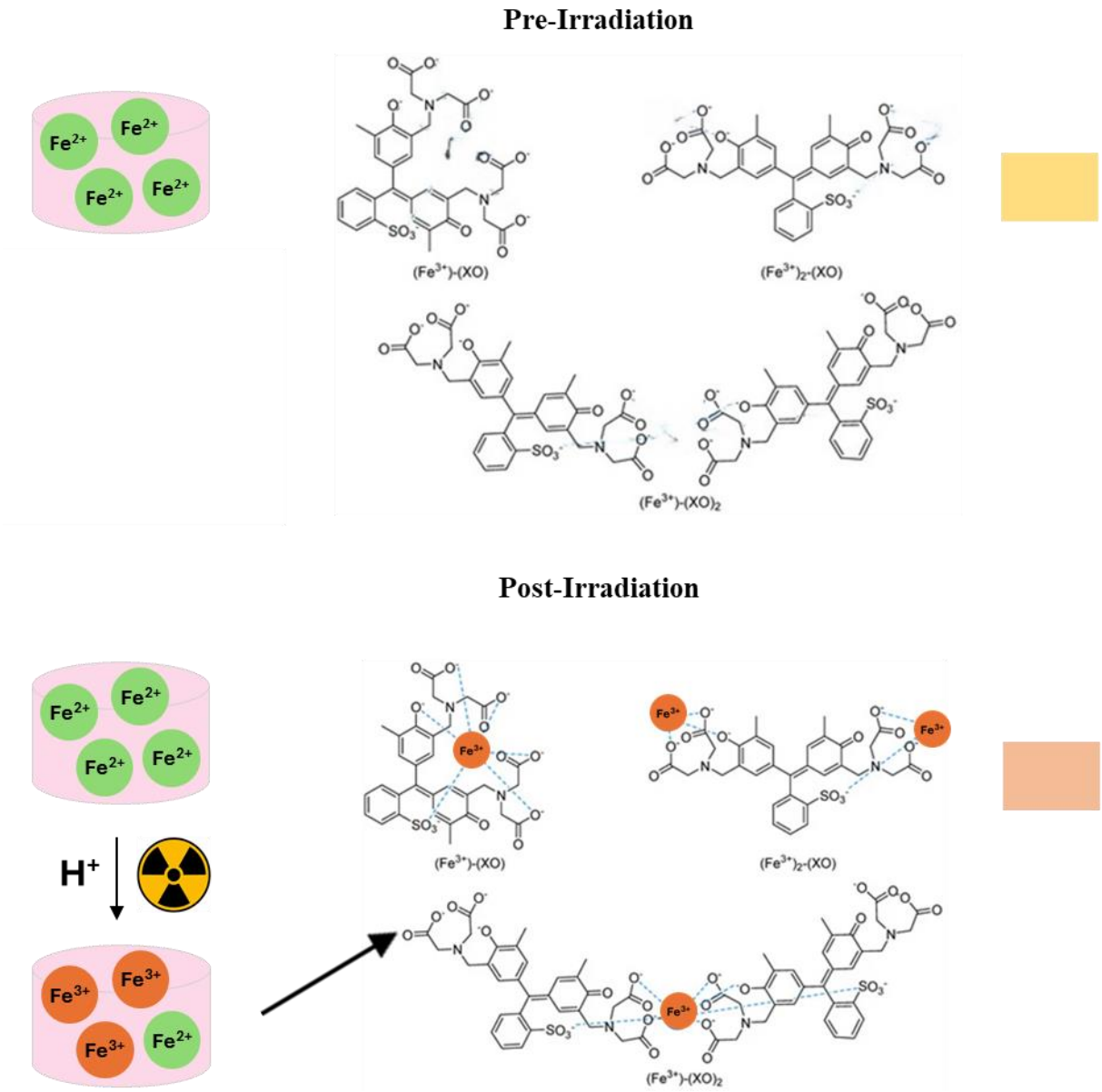


*Figure 2*. Hydrogel Chemical Response to Radiation. A representation of the chemical change that Fricke xylenol orange dosimeter hydrogels undergo when exposed to radiation. Dosimeter hydrogels pre-irradiation have $Fe^{2+}$ ions. These ions cannot bind to Xylenol Orange. After the hydrogel receives radiation, $Fe^{2+}$ can be oxidized to $Fe^{3+}$, which can bind to Xylenol Orange, inducing a color change.

Seminal studies have determined that the following concentration ranges of these components work best within gelatin-based hydrogels for measuring radiation: 0.4-1 mM Mohr's Salt, 25-50 mM sulfuric acid, and 0.15-0.2 mM Xylenol Orange. [54,56,58–70] A properly optimized gel can then be scanned with MRI. When a small part of the gel becomes irradiated, this area will increase in magnetic resonance proportionally to the amount of radiation that it receives.[54,56,58–70] The end-product is a 3-D reconstructed map of the gel. It should display how much radiation each area of the gel received during irradiation.[46,71]

For a time, gelatin was the gold standard of gel dosimetry and there was interest in being able to use such dosimeters to verify clinical radiation treatments of cancer patients. However, while it was a popular subject of dosimetry research for many years, it suffered from fast diffusion rates of ferric ions. For *in vivo* dosimetry, an additional challenge is that gelatin gels do not remain solid at body temperature.[56,65,72–74] In fact, while these hydrogels are quite efficient and accurate at measuring radiation, they cannot be used clinically since they cannot function at body temperature. As a result, there have been no animal studies conducted with dosimeter hydrogels. As old gelatin based "Fricke gels" failed to evolve beyond *in vitro* studies, there is a need to incorporate Fricke components to other hydrogel chemistries that are stable at body temperature.

### 1.5 Injectable Hydrogels and Their Potential Use as Radiation Dosimeters

Injectable hydrogels are systems that can go from a solution to a gel *in situ* after injection. Injectable hydrogels usually have an activation method that causes physical or chemical crosslinking to occur. These catalysts can include changes in external factors such as temperature or pH.[75] There are many advantages of utilizing an injectable gel

system: they are minimally invasive, they reduce scarring, decrease risk of infection, and they are easy to deliver compared to traditional gels.[76,77]

There is interest in developing an injectable hydrogel with the ability to measure radiation. Hydrogels that utilize a click chemistry reaction between norbornene and tetrazine macromers are of great interest to advancing hydrogel dosimetry. These hydrogels form through a Diels-Alder reaction, where a polymer chain modified with norbornene encounters a polymer chain modified with tetrazine. The resulting reaction causes the various polymers to crosslink through an interaction between norbornene and tetrazine moieties.[78–80] In practice, these hydrogels would turn from a solution into a gel in just minutes. The hydrogels should also be able to remain solid at body temperature, making them an ideal candidate for *in vivo* dosimetry.

### 1.6 Hypothesis and Aims

Currently, no studies have attempted to characterize the dosimetric properties or capabilities of an injectable hydrogel loaded with dosimeter components that are stable at body temperature. The hypothesis of this work is that a self-forming, injectable hydrogel with dosimetric components will endow radiation oncologists with the ability to assess radiation as it is being delivered inside patients while receiving magnetic resonance-guided radiation treatment. To test this hypothesis, we developed an injectable hydrogel system consisting of a hyaluronic acid (HA) backbone modified with either Norbornene (Nor) or Tetrazine (Tet) moieties, loaded with Fricke components. These hydrogels are stable at room and body temperature, and we evaluated the dosimetric capabilities of these hydrogels, namely their sensitivity to radiation, assessed by a change in optical

density, and compared these novel hydrogels to traditional gelatin-based Fricke gel dosimeters.

# Chapter 2

# Synthesis and Characterization of Injectable Dosimeter Hydrogels at Room Temperature

## 2.1 Introduction

To our knowledge, Diels-Alder norbornene-tetrazine click chemistry has not been utilized towards developing injectable dosimeter hydrogels. Although the concentration of Fricke dosimeter components in gelatin-based dosimeter gels has been well documented and characterized,[54,56,58–70] due to the novelty of this platform we sought to study how systematically varying the concentrations of each Fricke component affect dosimeter sensitivity. Sulfuric acid stabilizes and halts oxidation reactions of ferrous ions in the absence of radiation, allowing for more accurate readings. Xylenol orange is a chelating agent that allows us to determine the dose of radiation the dosimeter hydrogel absorbed based on a color change that occurs when radiation oxidizes ferrous ions into ferric ions. Mohr's salt is the supply of ferrous ions, which are the most vital component for radiation dosimetry. All components must be tested and optimized to perform at room temperature. Once all aspects of the injectable dosimeter hydrogel have been optimized at room temperature, it should be compared directly to the previous gold standard of hydrogel dosimetry—gelatin-based Fricke hydrogels. Since gelatin Fricke hydrogels were once the pinnacle of hydrogel dosimetry, the results of this comparison determine if our injectable dosimeter hydrogel functions at an acceptable level.

## 2.2 Materials and Methods

### *2.2.1 Gelatin Hydrogel Dosimeter Formation*

Gelatin dosimeters were always made at 2% w/v. To make this hydrogel, we formed the Fricke solution and the gelatin solution, with no Fricke components, separately. In doing so, a solution containing the final volume was predetermined, where we put gelatin mix in a beaker and soaked it with 75% of the final volume. This beaker was then placed on a stir plate heated to 40°C and the solution was mixed thoroughly using a magnetic stir bar. The Fricke solution comprises 25% of the final volume of the gelatin solution. The Fricke components present here must be four times greater than the concentrations of the Fricke components planned for the final solution. When this is added to the gelatin solution, the dilution is 4:1. The Fricke solution was made one component at a time, and we vortexed the solution each time a new component was added. Once the Fricke solution was complete and added to the gelatin solution, we allowed the final solution to mix for 5 minutes before dispensing it to the proper storage mold. We then placed the storage molds in a 4°C refrigerator until the solution had completely gelled. This generally took from 30 minutes up to 2 hours depending on the size of the batch you place in the storage molds of choice. Gelation time increases with increasing hydrogel precursor batch size.

### *2.2.2 Injectable Dosimeter Hydrogel Formation*

HANor-HATet dosimeters were always made at 2% w/v. To make this hydrogel, we needed to make two separate solutions: an HANor solution and an HATet solution. To create the HANor, solution, we dissolved HANor (2% w/v) in MilliQ water inside a small Eppendorf tube that was vortexed until the solution turned clear. It should be noted

that the amount of MilliQ water used is the amount of solution volume left that isn't comprised of the Fricke components. This was always calculated beforehand. The solution was then vortexed until the HANor macromer appeared to be completely dissolved. Next, we added the Fricke dosimeter components. It should be noted that our HANor solution is the only one that contained Fricke components. We added the Fricke components one at a time, vortexing the solution each time a new component was added. As a side note: we always recommend adding Mohr's salt last so that the Xylenol Orange doesn't end up "browning" in the process. It is crucial that the Fricke components present here be two times greater than the concentrations of Fricke components planned for the final HANor-HATet solution. When the HANor is added to the HATet, the dilution of the Fricke components is 2:1. However, it should be noted that this logic does not apply for HANor and HATet macromers. When the two components are added together, we consider them to be the same polymer. Therefore, if you add a solution that contains 2% HANor to a solution that contains 2% HATet, the final solution will be considered to have 2% HANor-HATet w/v overall. Following this, we would make our HATet solution. We would add an amount of the HATet macromer into a small Eppendorf equivalent to 2% w/v of the final HATet solution. We would then add an amount of MilliQ water equivalent to the total solution volume of the HANor solution as these two volumes should match. Following this step, we vortexed the solution until the HATet appeared to completely dissolve. Lastly, we would add an amount of HANor to a separate Eppendorf followed by adding an equivalent amount of HATet to that same Eppendorf to initiate the mixing process via micropipette. It is important to note that once this was done, we only had 5 minutes to mix the two solutions together via micropipette and then

dispense it to a mold/container. After 5 minutes the HANor-HATet solution should have solidified into a hydrogel.

### *2.2.3 Measuring Optical Density via Spectrophotometry*

In dosimetry, changes in the visible light spectrum of the gels are one way of determining sensitivity to radiation. Dosimeters are loaded with $Fe^{2+}$ and Xylenol Orange. When the gels are irradiated, it causes a reaction that oxidizes $Fe^{2+}$ to $Fe^{3+}$. When this occurs, $Fe^{3+}$ ions bind to Xylenol Orange structures, which cause a change in optical absorbance of a dosimeter gel. Normally, before there is a significant presence of Ferric ions in the gel, the dosimeter usually has an absorbance peak around 430 nm. However, after the gel is irradiated, there is an increase in optical absorbance at 585 nm proportional to the amount of radiation that the gel receives. This consequently causes a decrease in the optical peak observed at 430 nm.[67]

Optical scanning was performed with a SpectraMax iD5. The machine is connected to a laptop that contains the Softmax Pro software. For most studies, optical absorbance was scanned between light wavelengths of 360 nm to 720 nm.

### *2.2.4 Irradiating Hydrogel Samples with LINAC*

Hydrogel samples were contained in 96 well plates and irradiated from anywhere between 0 MU to 4000 MU, which equates to approximately 0 Gy to 40 Gy, respectively. All samples were irradiated with a LINAC on site at MD Anderson Cancer Center at Cooper in Camden, New Jersey. The field size used was 20 cm by 20 cm due to the size of the 96 well plates used to contain the hydrogel samples. The energy used was 15 MeV.

### *2.2.5 Statistics*

Statistical analysis was performed using GraphPad Prism (version 10.3.0, GraphPad software, Inc., La Jolla, CA). All experiments were carried out in triplicate. Analysis of variance (ANOVA) was performed followed by Tukey's test for post-hoc analysis. Differences among groups are stated as $p < 0.05$ (*), $p < 0.01$ (**), $p < 0.001$ (***), and (ns) when differences between groups are not statistically significant.

## 2.3 Results and Discussion

### *2.3.1 Xylenol Orange and Sulfuric Acid Characterization of a Protype Dosimeter: Initial Testing*

The first experiment we did was an attempt to optimize both Xylenol Orange and sulfuric acid for the first use of the HANor-HATet hydrogel. While we had some preliminary data on this, we decided to retest all parameters. The test parameters for these initial studies are presented in Table 1 and Table 2.

**Table 1**

*List Xylenol Orange (XO) Solutions Used in Initial Optical Density Readouts*

| Sample | XO Solution Concentration (mM) |
|---|---|
| A | 0.5 |
| B | 0.2 |
| C | 0.15 |
| D | 0.1 |
| E | 0 |

**Table 2**

*List of Hydrogel Components used in Initial Optical Density Readouts*

| 2 wt % Nor-Tet | XO (mM) | Acid (mM) | Mohr's (mM) |
|---|---|---|---|
| GA | 0.05 | 10 | 1 |
| GB | 0.05 | 25 | 1 |
| GC | 0.2 | 10 | 1 |
| GD | 0.2 | 25 | 1 |

(a)

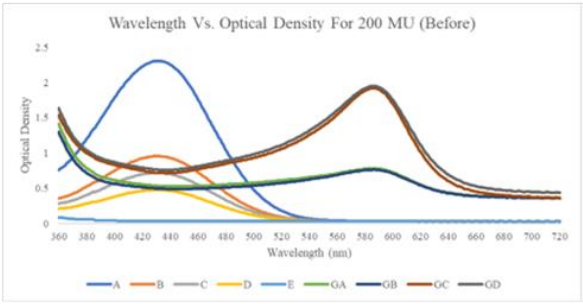


(b)

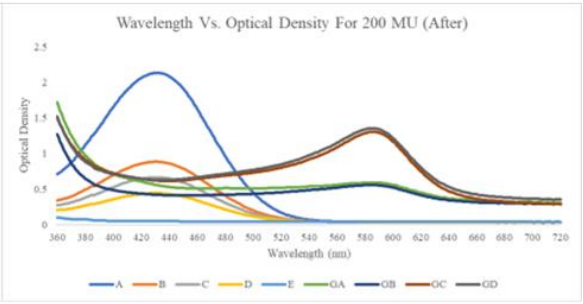


(c)

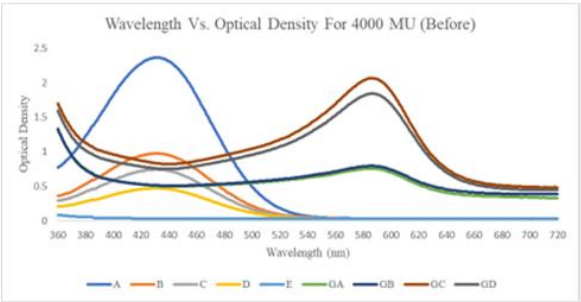


(d)

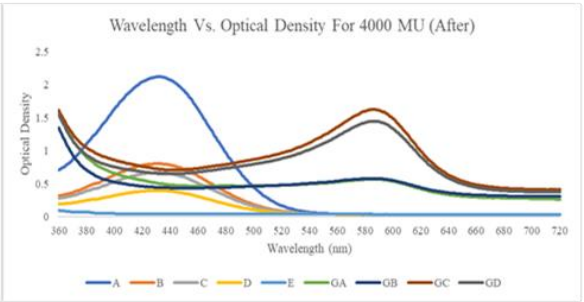


(e)

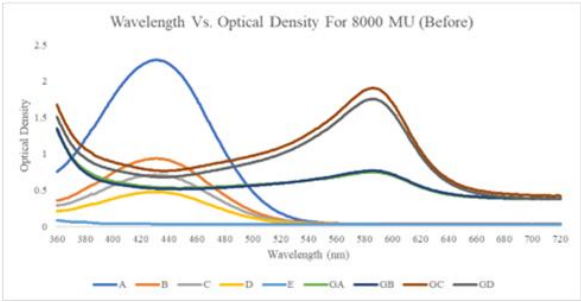


(f)

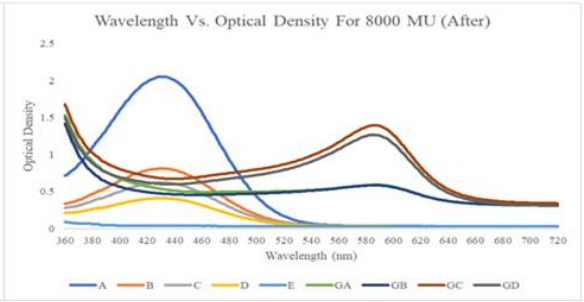

*Figure 3*. Initial HANor-HATet Hydrogel Dosimeter Characterization Via the Modulation of Xylenol Orange and Sulfuric Acid. Optical Density Readings obtained through spectrophotometric analysis. (a) Optical readouts of a well plate containing samples before receiving 200 MU of radiation. (b) Optical readouts of a well plate containing samples After 200 MU of radiation. (c) Optical readouts of a well plate containing samples before receiving 4000 MU of radiation. (d) Optical readouts of a well plate containing samples After 4000 MU of radiation. (e) Optical readouts of a well plate containing samples before receiving 8000 MU of radiation. (f) Optical readouts of a well plate containing samples After 8000 MU of radiation.

Although these initial tests did not go as planned, we learned that HANor-HATet hydrogels containing higher concentrations of Xylenol Orange appeared to display higher optical densities, which we surmised would lead to higher radiation sensitivities (Figure 3 a-f). As evident by the data, the optical density of the hydrogels decreases after being irradiated. It was expected that after irradiation, the optical density of each sample would increase proportionally with the amount of radiation received.

In hindsight, the reason that these experiments did not go as planned is most likely due to the improper vortexing of HANor and HATet solutions before mixing and gelling. As we understand at this point, sulfuric acid is a component used to stabilize a dosimeter hydrogel, preventing the self-oxidation of any ferrous ions into ferric ions. What happened in this case is that the sulfuric acid was not distributed properly within the hydrogel, causing spontaneous and rapid self-oxidation of ferrous ions into ferric

ions. This led to all Xylenol Orange in the solution being used up in an instant, and as a result, no further ferric ion to Xylenol Orange bonding could occur, leading to a loss of optical density over time. This is made further evident by the purple color that the HANor-HATet hydrogels took on almost immediately. Although, this revelation would not become clear until later testing.

### *2.3.2 Sulfuric Acid Optimization at Room Temperature*

We next wanted to aim for a successful sample irradiation test. At this point we felt confident with consistently using 0.2 mM Xylenol Orange and 1 mM Mohr's salt for all samples going forward. The aim of the next experiment was to evaluate the role of sulfuric acid concentration on change in optical density. Again, we tested both aqueous Fricke and HANor-HATet hydrogels.

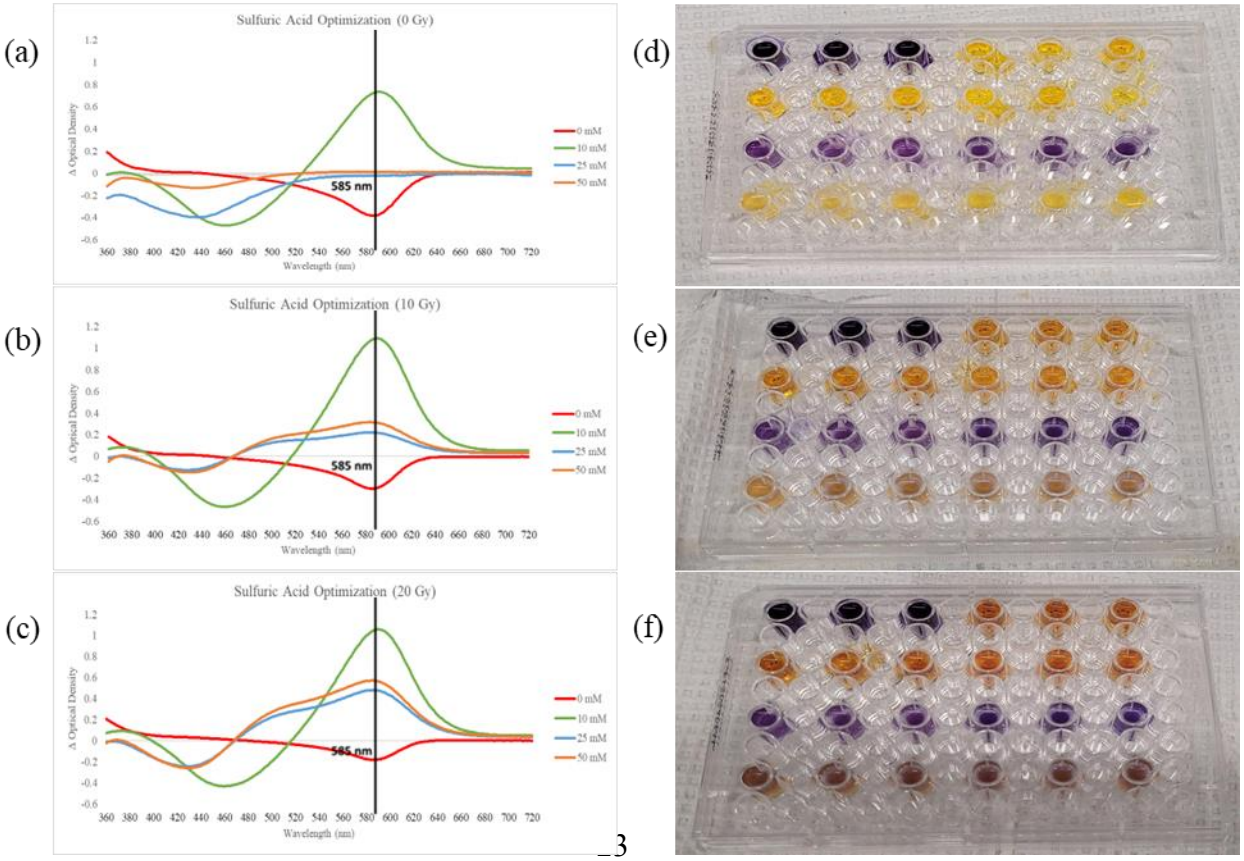

*Figure 4*. Broad Sulfuric Acid Optimization at Room Temperature. Optical density readings obtained through spectrophotometric analysis. (a) Depicts the change in optical density of the dosimeters after receiving no radiation. (b) Depicts the change in optical density of the dosimeters after receiving 10 Gy of radiation. (c) Depicts the change in optical density of the dosimeters after receiving 20 Gy of radiation. (d) Visual of a sample plate that received 0 Gy of radiation. (e) Visual of a sample plate that received 10 Gy of radiation. (f) Visual of a sample plate that received 20 Gy of radiation.

This experiment yielded successful results as the improper vortexing issue previously discussed was discovered and corrected. As expected, with what we understood about sulfuric acid at the time, the samples with 0 mM sulfuric acid lost optical density after irradiation. The samples with 10 mM sulfuric acid had the highest gain in optical density with every dose of radiation. The samples containing 25 mM and 50 mM sulfuric acid seemed to have similar gains in optical density across all doses of radiation (Figure 4 a-c).

Upon first inspection, it appears that the samples containing 10 mM sulfuric acid had the best sensitivity to radiation. However, this is not the case. Across both doses of radiation, the 10 mM sulfuric acid samples have the same gain in optical density of approximately 1 AU. Furthermore, unirradiated samples experience a large gain in optical density, lending more credence to our thoughts that sulfuric acid is used to curb self-oxidation of ferrous ions. In fact, the reason that the 0 mM sulfuric acid samples probably ended up losing optical density after irradiation is because all Xylenol Orange molecules were likely bonded to ferric ions instantly upon the addition of the Mohr's salt.

This would once again lead to the gradual decrease in optical density that was observed across all doses of radiation that these samples received. However, samples that had 25 mM sulfuric acid and up had great sensitivity and an almost proportional response to the dose they were given. It could be that at a minimum, the required amount of sulfuric acid to prevent obstructive amounts of self-oxidation is 25 mM. This is generally a trend that we have observed in many other studies regarding dosimeter hydrogels as well.[54,64,66,68,70]

We wanted to test this further by looking at a smaller concentration range of sulfuric acid: 10, 15, 20, and 25 mM. Our objective here was to examine if there was some range between 10 mM and 25 mM sulfuric acid that would be suitable in curbing the self-oxidation that we observed. We also wanted to add some longevity studies to see how our hydrogels would maintain dosimetric properties over time, with or without receiving doses of radiation.

From the data, it appears that the 10 mM sulfuric acid samples that were unirradiated follow the same trend as previously reported: it reaches a maximum gain in optical absorbance and then slowly starts to lose optical density over time. The 15 mM samples had a small amount of self-oxidation without receiving radiation initially. Over the course of 1 day these samples gained a considerable amount of optical density, reaching almost 1 AU for samples that are unirradiated and 1.4 AU for samples that receive 20 Gy. The 20 mM samples follow a somewhat similar trend, albeit one day delayed. They start out with an identical radiation sensitivity curve immediately after irradiation. At 10 Gy, they reach approximately 0.25 AU. At 20 Gy, they reach an optical density of approximately 0.5 Gy. However, after 1 day following irradiation, all unirradiated and irradiated samples gain approximately 0.3 AU optical density. For the 25

mM sulfuric acid samples, they show a strong linear response to radiation. Furthermore, these samples also have a significantly lower gain in optical density than the samples containing the next lowest amount of sulfuric acid—15 mM. Out of all samples, the 25 mM sulfuric acid group seems to have the best maintained dosimetric properties (Figure 5).

(a)

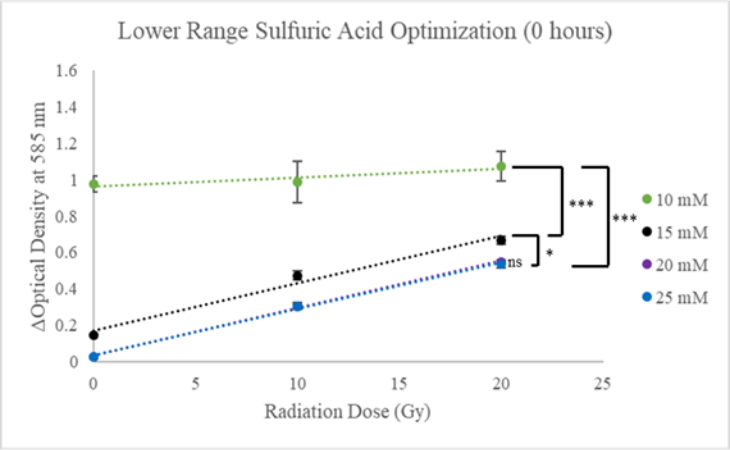


(b)

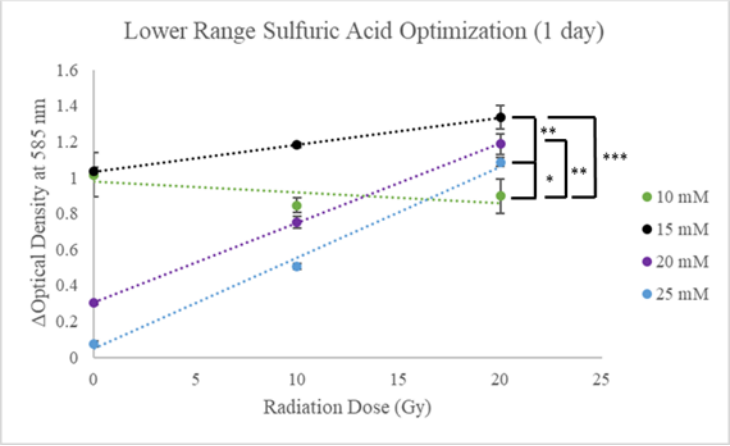

*Figure 5*. Lower Range Sulfuric Acid Optimization at Room Temperature. Depicts the change in optical density of the dosimeters after receiving 0 Gy, 10 Gy, and 20 Gy of radiation for two timepoints. All timepoints are measured in terms of time after the samples received radiation. All samples consist of 2% weight Nor-Tet, 1 mM Mohr's Salt and 0.2 mM Xylenol Orange. (a) Represents samples immediately after irradiation. (b) Represents samples 1 day after irradiation.

Most of the trends seen in this data set are completely within the realm of expectations based on previous experiments. It appears that when samples of any concentration of sulfuric acid reach their peak gain in optical density, they then begin to lose said optical density. The mechanisms as to why this occurs remain unknown at the moment, but it cannot be denied that it is a consistent occurrence. Perhaps, this may be caused by the diffusion of both $Fe^{2+}$ and $Fe^{3+}$ ions within the matrix, causing the destruction of optical information, leading to a loss in optical density as a result.[54] Though, that is just speculation at this juncture.

To continue studying the effects of sulfuric acid concentration on radiation sensitivity in our HANor-HATet dosimeter hydrogels, a wider range of Sulfuric Acid concentrations were tested. The concentrations tested are as follows: 25 mM, 50 mM, and 100 mM. This study only focused on the change in optical absorbance from before irradiation to immediately after irradiation, and from before irradiation to 1 day after irradiation.

(a)

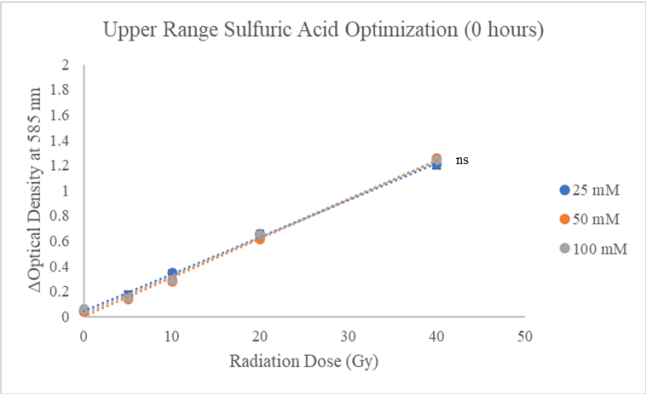


(b)

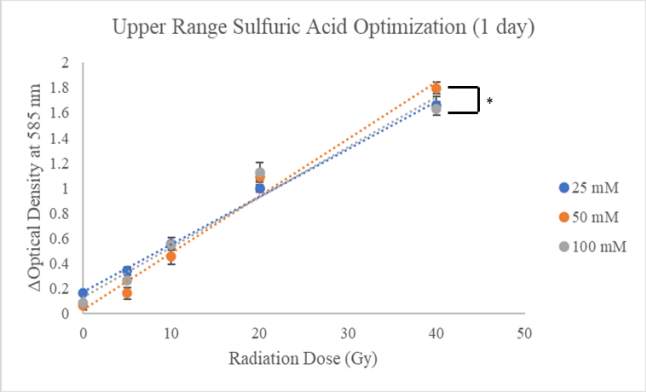


*Figure 6*. Upper Range Sulfuric Acid Optimization. Depicts the change in optical density of the dosimeters after receiving 0 Gy, 5 Gy, 10 Gy, 20 Gy, and 40 Gy of radiation for two timepoints. All timepoints are measured in terms of time after the samples received radiation. All samples consist of 2% weight Nor-Tet, 1 mM Mohr's Salt and 0.2 mM Xylenol Orange. (a) Represents samples immediately after irradiation. (b) Represents samples 1 day after irradiation.

The data shows that all three sample groups have an identical sensitivity to radiation. All unirradiated samples have an optical density gain close to 0 AU

immediately following irradiation. After receiving 5 Gy, all samples display an optical density gain of approximately 0.15 AU. At 10 Gy, all samples display an optical density gain of about 30. AU. After receiving 20 Gy, all samples seem to have gained 60 AU in terms of optical density. Samples that received 40 Gy see an optical density change of about 1.2 AU (Figure 6a). After 1 day, it seems that dosimetric properties are relatively maintained across all groups. There were gains in optical density across all groups from the previous day (Figure 6b).

Overall, these results show that in the case of HANor-HATet, increasing the concentration of sulfuric acid beyond 25 mM has no effect on either radiation sensitivity or on maintaining dosimetric properties. Some studies suggest that an excess of sulfuric acid decreases radiation sensitivity.[54] Our long-term goal is to use this hydrogel *in vivo*, and thus we want to use as low of a sulfuric acid concentration as possible. Since there is no clear benefit in raising the sulfuric acid concentration past 25 mM, we choose 25 mM as our optimized concentration for the HANor-HATet dosimeter.

### *2.3.3 Mohr's Salt Optimization at Room Temperature*

To further optimize the HANor-HATet dosimeter, a wider range of Mohr's Salt concentrations were tested. The concentrations tested are as follows: 0.1 mM, 0.5 mM, 0.75 mM, and 1 mM. This study only focused on the change in optical absorbance noted from before irradiation to immediately after irradiation, and from before irradiation to 1 day after irradiation.

(a)

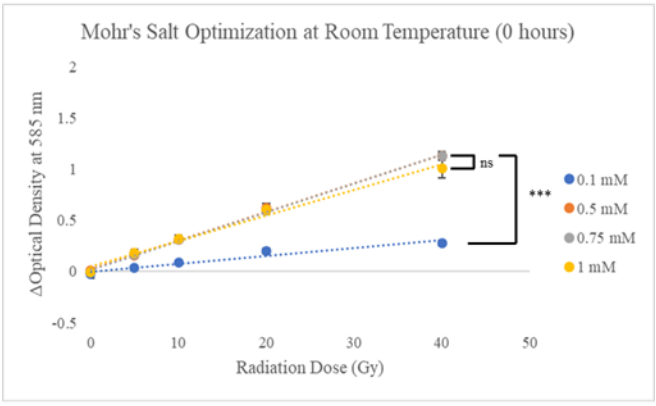


(b)

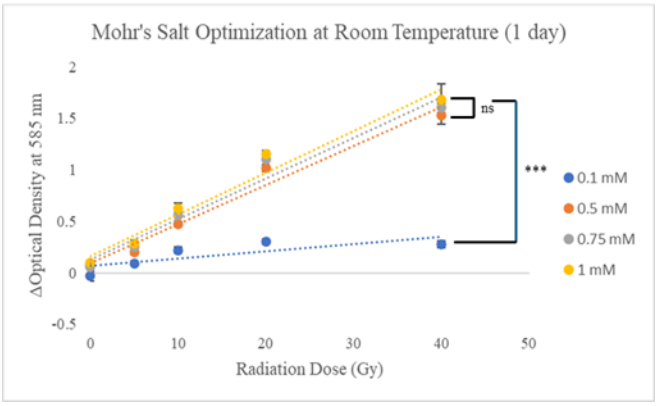


*Figure 7*. Optimization of Mohr's Salt at Room Temperature. (a) Represents HANor-HATet samples containing 0.1 mM, 0.5 mM, 0.75 mM, and 1 mM Mohr's salt. All groups are kept at room temperature and read immediately after irradiation. (b) Represents HANor-HATet samples containing 0.1 mM, 0.5 mM, 0.75 mM, and 1 mM Mohr's salt. All groups are kept at room temperature and read 1 day after irradiation.

Immediately following irradiation, all samples in exception to the 0.1 mM group seem to have an identical sensitivity to radiation. In fact, the 0.1 mM group is hindered to such a degree by the drop in Mohr's salt, that it doesn't gain optical density past

approximately 0.3 AU. All other sample groups are not impacted by lower amounts of Mohr's salt. The 1 mM group does have one point lower than the other groups at 40 Gy; however, this is not a significant difference (Figure 7a).

There is an observable trend that samples containing lower concentrations of Mohr's Salt seem to retain their dosimetric properties slightly better than those containing higher concentrations. Although, this difference is not shown to be significant in these conditions. For samples containing 0.1 mM, their sensitivity seems lower than samples containing higher concentrations as their change in optical absorbance never seems to reach above 0.2 AU for any dosage of radiation. Samples containing 0.5 mM Mohr's salt are generally able to reach the absorbance peak that samples with higher concentrations can reach. At 0, 5, 10, 20, and 40 Gy, the change in optical absorbance respectively measures as follows: 0.08, 0.2, 0.47, 1.02, and 1.53 AU. This configuration appears to be the most optimal as increasing concentrations consistently correlate with higher changes in optical absorbance, indicating higher rates of self-oxidation. Although, the differences between the 0.5 mM group, the 0.75 mM and 1 mM groups are not very significant. The largest difference in usable concentrations is between the 0.5 mM and 1 mM groups. At 0, 5, 10, 20, and 40 Gy, the change in optical absorbance respectively measures as follows: 0.09, 0.28, 0.63, 1.15, and 1.68 AU (Figure 7b).

Overall, it seems that at the minimum, all HANor-HATet dosimeters must have a Mohr's concentration equivalent to or greater than 0.5 mM. Any lower concentration may result in a loss of dose sensitivity, as supported by other works.[67] Taking all data into account, it was decided that 1 mM is optimal for now. This was primarily decided due to

there being no discernible difference in the maintenance of dosimetric properties among the 0.5 mM, 0.75 mM, and 1 mM groups 1 day following irradiation.

### *2.3.4 HANor-HATet Hydrogel vs. Gelatin Hydrogel Dosimeters*

To compare both the HANor-HATet and the Fricke Gel dosimeter (Gelatin), both gels were prepared at 2% w/v ratio, with 0.2 mM Xylenol Orange, 25 mM Sulfuric Acid, and 1 mM Mohr's Salt. Samples were prepared in 96 well plates, using 100 µL per well and 230 µL of distilled water to top off the wells. All samples were then irradiated at room temperature utilizing a LINAC machine and promptly scanned using a plate reader.

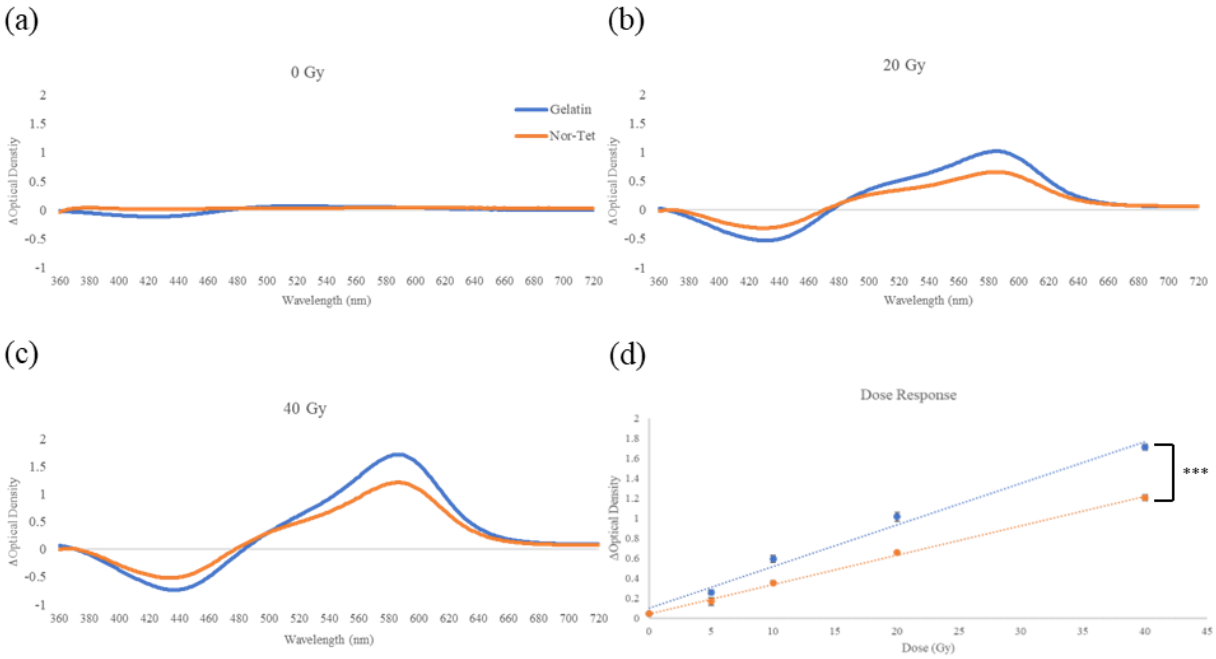


*Figure 8*. Gelatin vs. HANor-HATet Hydrogel Dosimetry Sensitivity Comparison. Demonstrates a comparison of dose sensitivity between gelatin Fricke and HANor-HATet hydrogels. All hydrogels utilize concentrations of 0.2 mM Xylenol Orange, 25 mM

sulfuric acid, and 1 mM Mohr's salt. (a, b, c) Shows the sensitivity of the gelatin and HANor-HATet gels, respectively, in terms of optical density measured between 360-720 nm. It was determined that reading at 585 nm is optimal for testing Fricke gel dose sensitivity. (d) Directly compares the linear dose response of gelatin Fricke and HANor-HATet hydrogels.

The HANor-HATet and Gelatin both displayed similar sensitivities to radiation. Although, it appears that Gelatin is consistently more sensitive to radiation than HANor-HATet by a small margin ($p < 0.0001$). At 0 Gy, it appears that both gels appear to have the same change in optical density at 585 nm, meaning that their self-oxidation rate is indiscernible from one another only after a few hours. This change in optical absorbance is noted to be approximately 0.04 AU (Figure 8a). When irradiated with a dose of 20 Gy, there is a small difference between the two samples, with Gelatin seeing a higher change in optical absorbance, 1.01 AU, than HANor-HATet, 0.65 AU, at 585 nm (Figure 8b). This trend continues when both gels are irradiated with 40 Gy. Gelatin sees a change in optical absorbance of 1.7 AU while HANor-HATet sees a change of 1.2 AU (Figure 8c). When the dose responses are plotted, they display a very strong linear response. It is also demonstrated that Gelatin is more sensitive than the HANor-HATet, especially beyond a dose of 10 Gy (Figure 8d).

Ultimately, the gelatin dosimeter being more sensitive to radiation than the HANor-HATet dosimeter could be a matter of the gelatin having a more cohesive matrix structure. HANor-HATet hydrogels have nitrogen bubbles form within their matrix upon gelation. It is stated that most dosimeters need sufficient oxygen to function properly.[61,68]

It could be possible that the nitrogen evolution within the HANor-HATet dosimeter which form the nitrogen bubbles purge the hydrogel of a significant amount of oxygen, ultimately leading to it being a less sensitive dosimeter than the gelatin. However, data still presents that the HANor-HATet dosimeter is still more than viable enough to use as a dosimeter. While there is a significant difference between HANor-HATet and gelatin in terms of radiation sensitivity, our data still suggests that the injectable is still more than usable, especially when compared to gelatin dosimeters that have been nitrogenated.[61] It is not the most ideal scenario, however, the HANor-HATet is still distinguishable enough at different doses of radiation to be reliable as a dosimeter.

### *2.3.5 Miscellaneous Characterization of Optical Density Trends*

Upon seeing that HANor-HATet dosimeters tended to be darker in appearance than gelatin Fricke, leading to a higher starting optical density, we decided to investigate what the cause of this could be. In this study, we wanted to investigate the impact of the macromer/polymer alone on the optical density, the impact of implementing Xylenol Orange into the hydrogels on optical density, and the impact of adding all Fricke components into the hydrogels on optical density. In doing so, we tested 9 different sample groups that are listed in Table 3. The concentrations of the Fricke components, when they were utilized in the hydrogels, are as follows: 0.2 mM Xylenol Orange, 25 mM sulfuric acid, and 1 mM Mohr's salt.

**Table 3**

*Conditions used to Determine Cause of HANor-HATet Hydrogel Dosimeter High Optical Absorbance*

| | | |
|---|---|---|
| HANor | HANor w/XO | HANor Dosimeter |
| HATet | HATet w/XO | HATet Dosimeter |
| HANor-HATet | HANor-HATet w/XO | HANor-HATet Dosimeter |
| Gelatin | Gelatin w/XO | Gelatin Dosimeter |

(a)

(b)

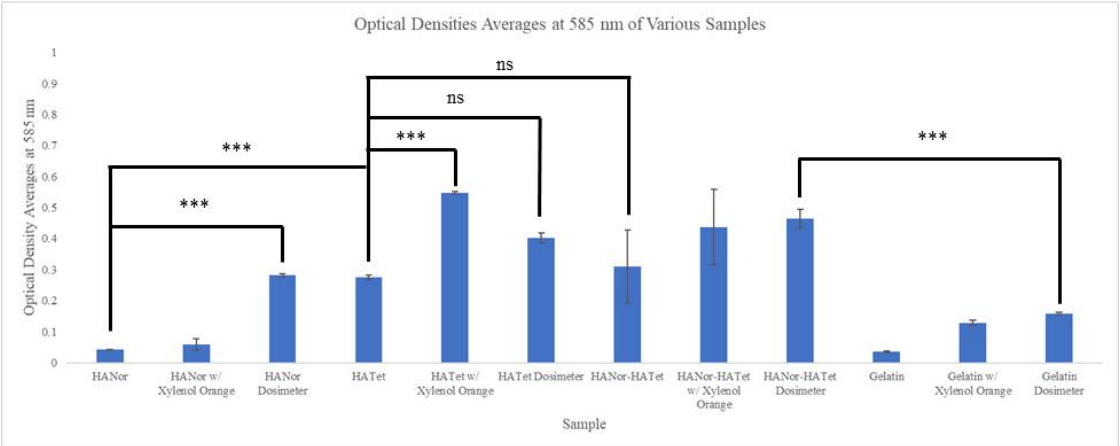

*Figure 9*. Optical Density Factor Experiment. A test to determine the factors behind the HANor-HATet's higher starting optical density over gelatin Fricke. (a) Picture visually displaying the colors of the different groups of hydrogels. Table 3 can be used as a reference to distinguish which groups are being displayed on the plate. (b) Displays the optical densities of all sample groups.

The HANor samples have a relatively low starting optical density as it appears as a clear, transparent liquid. Contrary to expectations, adding Xylenol Orange to the HANor alone did not significantly raise its optical density. However, when all Fricke components are added to the HANor solution, it jumps from approximately 0.05 AU to 0.275 AU. When analyzing the HATet solutions, which appear as a dark pink color without any Fricke components, it has an optical density of approximately 0.275 AU, which is very similar to the HANor with all Fricke components. Unlike the HANor samples, the HATet samples gain significant optical density when Xylenol Orange is added, increasing from approximately 0.3 AU to approximately 0.55 AU. However, when all dosimeter components are added, its optical density drops down to approximately 0.4 AU. The HANor-HATet samples without any Fricke components start at approximately 0.3 AU, which is similar to HATet without any Fricke components. When Xylenol Orange is added, the sample's optical density equates to approximately 0.425 AU. After all Fricke components are added to the HANor-HATet, sample optical density increases to approximately 0.45 AU. The gelatin samples follow a similar trend as the HANor-HATet samples, though with lower overall optical densities. The gelatin samples without any Fricke components start at approximately 0.025 AU. Gelatin samples' optical density

increases to approximately 0.125 AU when Xylenol Orange is added and to approximately 0.15 AU when all Fricke components are in the gelatin (Figure 9).

It appears that the HATet is the primary factor as to why the HANor-HATet dosimeters have such a high starting optical density compared to gelatin. Indicators of such a conclusion are evident when comparing the HANor dosimeter samples to HA-Tet and HANor-HATet samples without any Fricke components. HATet's starting optical density without any dosimeter components is almost identical to the HANor dosimeter. Moreover, the HANor-HATet samples without any Fricke components seem to have a similar optical density to the HATet samples without any Fricke components. By this logic, we can conclude that the significant difference between the starting optical densities of HANor-HATet dosimeters and gelatin Fricke is primarily caused by the HATet. Since HANor is a colorless, clear liquid it does not contribute much to the overall optical density that is common of the HANor-HATet dosimeter. However, since HATet is a dark pink color, this is more than likely a major contributor to HANor-HATet's higher optical density compared to the gelatin Fricke. It appears that other factors may still contribute to the injectable dosimeter's higher optical density though.

Next, we commenced a more thorough study of the effects of dosimeter components on the optical density of the HANor-HATet hydrogel. More specifically, this study comprises of HANor-HATet hydrogels with Xylenol Orange in every sample group. We already understand that Xylenol Orange is a contributing factor to the increased optical density seen in hydrogel samples previously. We wanted to use it as a reference in this experiment. We tested HANor-HATet groups with Xylenol Orange alone, with Xylenol Orange and sulfuric acid, and with Xylenol Orange and Mohr's salt.

(a)

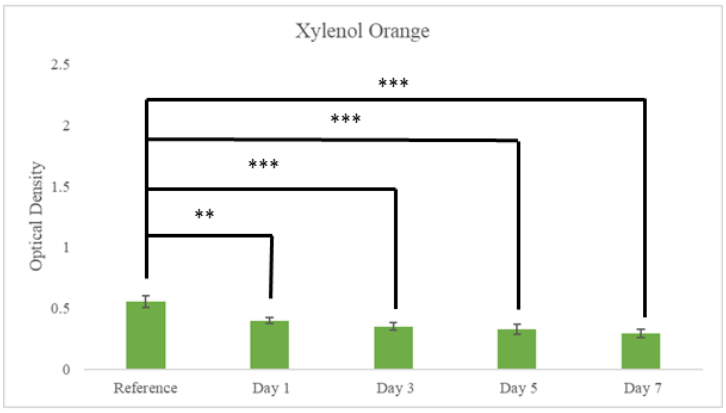


(b)

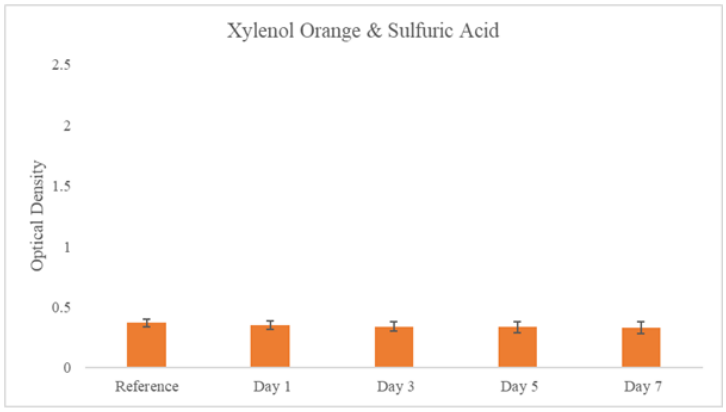


(c)

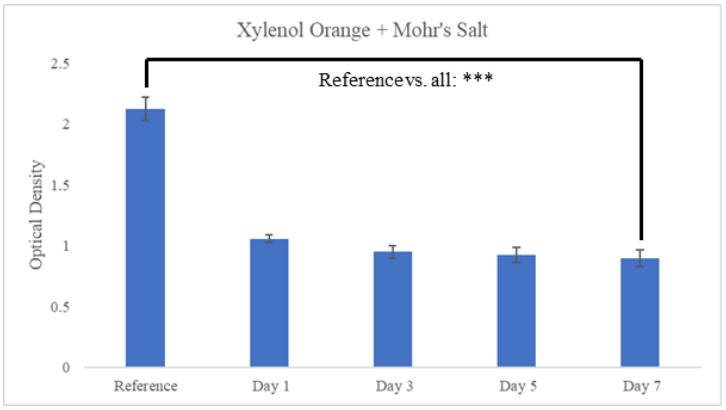


*Figure 10*. Dosimeter Component Effect on HANor-HATet's Optical Density. "Reference" refers to day 0. (a) A seven-day study performed on HANor-HATet containing only Xylenol Orange. Optical density is measured at 585 nm. (b) A seven-day

study performed on HANor-HATet containing both Xylenol Orange and sulfuric acid. Optical density is measured at 585 nm. (c) A seven-day study performed on HANor-HATet containing both Xylenol Orange and Mohr's salt. Optical density is measured at 585 nm.

The Xylenol Orange samples start at an optical density of approximately 0.5 AU on the reference day, which is also known as day 0. The samples lose optical density between the reference day and day 1, dropping to approximately 0.4 AU. From this point on, the optical density drops slowly until it reaches approximately 0.3 AU on day 7 (Figure 10a). The Xylenol Orange and sulfuric acid samples begin with an optical density of 0.4 and remain relatively stable over the course of the 7 days (Figure 10b). The Xylenol Orange and Mohr's salt samples begin at approximately 2.1 AU. By day 1, it quickly lowers to approximately 1 AU and down to approximately 0.9 AU by the end of 7 days (Figure 10c).

As expected, samples containing only Xylenol Orange are relatively stable. However, it is interesting to note that these samples see a small and steady decrease in their optical densities over time. Perhaps Xylenol Orange once put into a hydrogel begins to slowly lose optical density over time due to diffusion. Such a hypothesis will require more testing though. Interestingly, samples with Xylenol Orange and sulfuric acid appear to start at a lower optical density than samples with just Xylenol Orange and remain stable for the entirety of the week. Ultimately, sulfuric acid does not contribute to the higher optical density of the samples seen previously. The Xylenol Orange and Mohr's salt samples have a starting optical density of 2.1 AU, implying that the dosimeter has

reached peak absorbance based off previous experiments. It quickly drops to approximately 1 AU and continues to decline to 0.9 over the course of the week. Overall, when comparing hydrogels without Fricke components and hydrogels with Fricke components, it appears that the two contributing factors of a dosimeter hydrogel's higher optical density are Xylenol Orange and Mohr's salt.

### 2.4 Conclusions

The aim this study set out to accomplish was to optimize dosimetry components in HANor-HATet dosimeters. After extensive studies and experiments, we concluded that at room temperature, the optimal concentrations of standard dosimetry components are as follows: 0.2 mM Xylenol Orange, 25 mM sulfuric acid, and 1 mM Mohr's salt. Of all tested concentrations, these consistently gave us the radiation sensitivity for the HANor-HATet hydrogels. Furthermore, HANor-HATet compares well to the previous gold standard of hydrogel dosimetry, gelatin Fricke. While gelatin has better overall sensitivity to radiation, it cannot be denied that much like gelatin Fricke, HANor-HATet dosimeters have a very linear and very distinct dose response. Taken altogether, this makes HANor-HATet a strong dosimeter that is ready for body temperature testing.

# Chapter 3

# Evaluating Change in HANor-HATet Hydrogel Optical Density as a Function of Radiation at Body Temperature

## 3.1 Introduction

In our last study, we did extensive work to characterize the HANor-HATet hydrogel as a dosimeter and compared our formulations to gelatin Fricke. Now that we have ensured that its dosimetric components are optimized, we want to test the HANor-HATet dosimeter at body temperature. We first want to ensure that it maintains dosimetric functionality at body temperature. If our hydrogel still proves to be functional at these conditions, then we intend to evaluate its change in optical density as a function of radiation at body temperature. If needed, we will investigate if further optimization of dosimetry components for HANor-HATet is possible.

## 3.2 Materials and Methods

### *3.2.1 Injectable Dosimeter Hydrogel Formation*

HANor-HATet dosimeters were always made at 2% w/v. To make this hydrogel, we needed to make two separate solutions: an HANor solution and an HATet solution. To create the HANor solution, we dissolved HANor (2% w/v) in MilliQ water inside a small Eppendorf tube that was vortexed until the solution turned clear. It should be noted that the amount of MilliQ water used is the amount of solution volume left that isn't comprised of the Fricke components. This was always calculated beforehand. The solution was then vortexed until the HANor macromer appeared to be completely dissolved. Next, we added the Fricke dosimeter components. It should be noted that our HANor solution is the only one that contained Fricke components. We added the Fricke

components one at a time, vortexing the solution each time a new component was added. As a side note: we always recommend adding Mohr's salt last so that the Xylenol Orange doesn't end up "browning" in the process. It is crucial that the Fricke components present here be two times greater than the concentrations of Fricke components planned for the final HANor-HATet solution. When the HANor is added to the HATet, the dilution of the Fricke components is 2:1. However, it should be noted that this logic does not apply for HANor and HATet macromers. When the two components are added together, we consider them to be the same polymer. Therefore, if you add a solution that contains 2% HANor to a solution that contains 2% HATet, the final solution will be considered to have 2% HANor-HATet w/v overall. Following this, we would make our HATet solution. We would add an amount of the HATet macromer into a small Eppendorf equivalent to 2% w/v of the final HATet solution. We would then add an amount of MilliQ water equivalent to the total solution volume of the HANor solution as these two volumes should match. Following this step, we vortexed the solution until the HATet appeared to completely dissolve. Lastly, we would add an amount of HANor to a separate Eppendorf followed by adding an equivalent amount of HATet to that same Eppendorf to initiate the mixing process via micropipette. It is important to note that once this was done, we only had 5 minutes to mix the two solutions together via micropipette and then dispense it to a mold/container. After 5 minutes the HANor-HATet solution should have solidified into a hydrogel.

### *3.2.2 Measuring Optical Density via Spectrophotometry*

In dosimetry, changes in the visible light spectrum of the gels are one way of determining sensitivity to radiation. Dosimeters are loaded with $Fe^{2+}$ and Xylenol

Orange. When the gels are irradiated, it causes a reaction that oxidizes $Fe^{2+}$ to $Fe^{3+}$. When this occurs, $Fe^{3+}$ ions bind to Xylenol Orange structures, which cause a change in optical absorbance of a dosimeter gel. Normally, before there is a significant presence of Ferric ions in the gel, the dosimeter usually has an absorbance peak around 430 nm. However, after the gel is irradiated, there is an increase in optical absorbance at 585 nm proportional to the amount of radiation that the gel receives. This consequently causes a decrease in the optical peak observed at 430 nm.[67]

Optical scanning was performed with a SpectraMax iD5. The machine is connected to a laptop that contains the Softmax Pro software. For most studies, optical absorbance was scanned between light wavelengths of 360 nm to 720 nm.

### *3.2.3 Irradiating Hydrogel Samples with LINAC*

Hydrogel samples were contained in 96 well plates and irradiated from anywhere between 0 MU to 4000 MU, which equates to approximately 0 Gy to 40 Gy, respectively. All samples were irradiated with a LINAC on site at Cooper University Hospital in Camden New Jersey. The field size used was 20 cm by 20 cm due to the size of the 96 well plates used to contain the hydrogel samples. The energy used was 15 MeV.

### *3.2.4 Body Temperature Testing Setup*

All samples irradiated at body temperature were first wrapped in foil and placed in a humidifier. The humidifier was made by placing soaked paper towels in a large Tupperware container and sealing it with the lid. This humidifier was then placed in a warm room (37°C) before being irradiated.

### *3.2.5 Cell Culture*

To evaluate biocompatibility of HANor-HATet hydrogels, these hydrogels, with varying concentrations of dosimeter components, were cultured in the presence of mammalian cells. Human mesenchymal stem cells (MSCs) were expanded on tissue culture plastic plates, and once cells reached 80-90% confluency, they were passaged, counted, and seeded on wells of a 24-well plate (5,000 cell/cm$^2$) in MSC culture medium (αMEM, 10% fetal bovine serum, 1% penicillin/streptomycin). MSCs were then exposed to HANor-HATet hydrogels using tissue culture plate inserts. HANor-HATet hydrogels were made using 8 mm diameter rubber molds and then promptly placed into an insert which would make direct contact with the MSC medium. MSCs were cultured in the presence of HANor-HATet hydrogels over the course of 7 days. Viability was evaluated at 1 day, 3 days, and 7 days after cells were initially cultured by measuring metabolic activity using an alamarBlue assay per manufacturer instructions. Using a micropipette, MSC culture medium was carefully removed from each well and replaced with 1 mL 10% alamarBlue in MSC culture medium. After replacement, the hydrogels were placed back into their appropriate wells. Well plates were incubated for four hours and before reading, the hydrogels were removed and placed in sterile PBS. The plates were read at a fluorescence wavelength of 570-610 nm.[81] After reading the plates, the alamarBlue medium was replaced with MSC culture medium, and the hydrogels were placed back in their original wells. The plates were then incubated until the next time point.

The standard curve used to correspond fluorescence with the number of live cells was developed by culturing a known number of cells into different wells. The number of cells used in each well was as follows: 0 cells, 5,000 cells, 10,000 cells, 15,000 cells, and

20,000 cells. When fluorescence of the wells was measured to develop the standard curve, each well contained alamarBlue in MSC culture medium.

### *3.2.6 Statistics*

Statistical analysis was performed using GraphPad Prism (version 10.3.0, GraphPad software, Inc., La Jolla, CA). Most experiments were carried out in triplicate. AlamarBlue experiments were carried out in sample sizes of n=9. Analysis of variance (ANOVA) was performed followed by Tukey's test for post-hoc analysis. Differences among groups are stated as $p < 0.05$ (*), $p < 0.01$ (**), $p < 0.001$ (***), and (ns) when differences between groups are not statistically significant.

## 3.3 Results and Discussion

### *3.3.1 HANor-HATet Hydrogel Dosimetry at Body Temperature*

To test the room temperature samples of HANor-HATet gels, the same procedure was used as mentioned for the previous test. For body temperature samples of HANor-HATet, all gels were made at room temperature, followed by being stored in a makeshift humidifier inside of a warm room for at least 30 minutes (Figure 11a, b, & c). All samples were irradiated by a LINAC machine and scanned using a plate reader. The concentrations for the dosimeter components used are as follows: 0.2 mM Xylenol Orange, 25 mM sulfuric acid, and 1 mM Mohr's salt.

(a)

(b)

(c)


*Figure 11*. Humidifier for Body Temperature Study. A visual of the humidifier used in the body temperature experiments. All samples irradiated at body temperature were first wrapped in foil, placed in the humidifier with soaked paper towels, then placed in a warm room (37°C) before being irradiated. (a) Tupperware container with 96-well plates inside.

(b) 96-well plates are wrapped in foil and surrounded by wet paper towels. (c) A lid is placed on the Tupperware container, making it a humidifier.

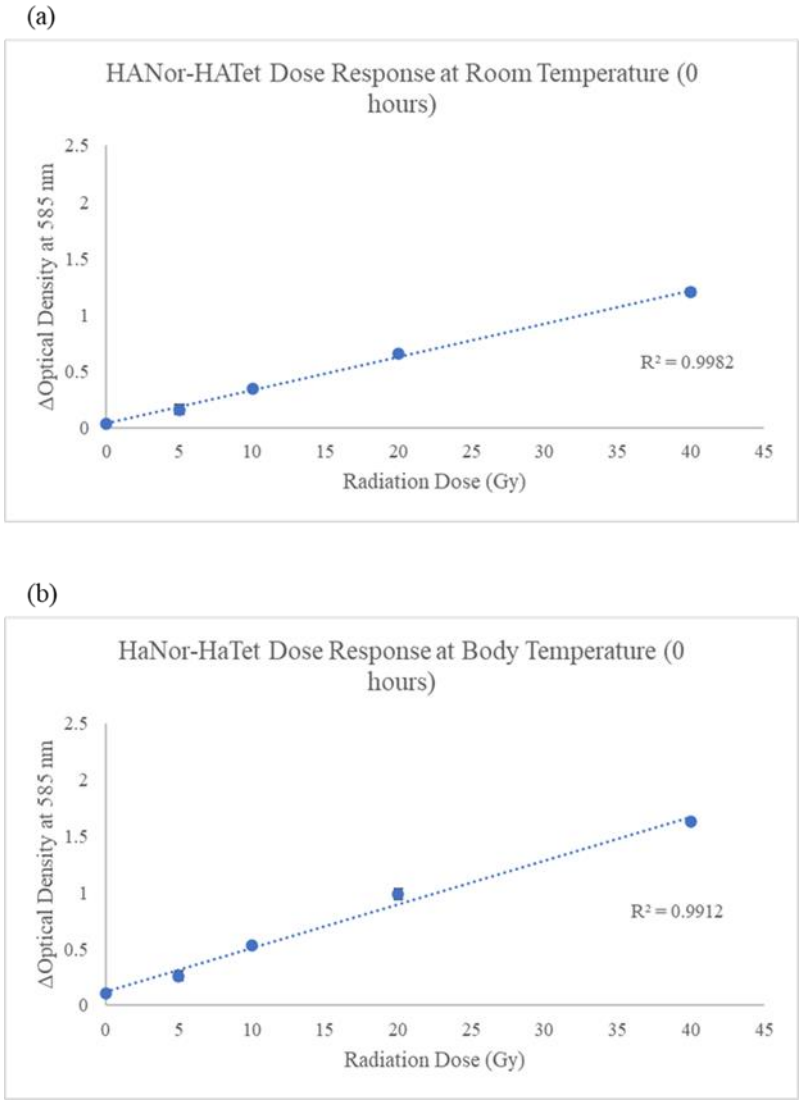


*Figure 12*. HANor-HATet Hydrogel Dosimeter: Room vs. Body Temperature. (a) Data for HANor-HATet hydrogels stored and irradiated at room temperature over the course of

one week. (b) Data for HANor-HATet hydrogels stored and irradiated at body temperature over the course of one week.

The room temperature samples showed similar results to previous experiments on the day of irradiation at all doses: 0 Gy, 5 Gy, 10 Gy, 20 Gy, and 40 Gy. The unirradiated samples seem to gain almost no optical density in the time between formation and sample irradiation. Further consistency can be observed with the samples irradiated with 40 Gy as, with the experiments prior to this, they only gained approximately 1.2 AU of optical density. (Figure 12a).

The data confirms that the HANor-HATet dosimeter will function at body temperature. Not only this, but the body temperature samples showed significantly higher sensitivity to radiation than room temperature samples, particularly with samples that received 20 Gy or higher. For reference, when comparing samples irradiated at 40 Gy between both groups, $p = 0.0037$. Furthermore, the data displays a strong correlation coefficient of 0.9912, suggesting that it remains a strong and reliable dosimeter (Figure 12b).

The HANor-HATet dosimeter being more sensitive to radiation at body temperature could be due to chemical reactions occurring faster at higher temperatures. It is well documented that increasing temperature increases reaction rates, and therefore, it is reasonable to correlate the increase from room to body temperature with the increase in sensitivity to radiation.[82] In fact, the increase in sensitivity in the HANor-HATet dosimeter makes it more comparable to the gelatin dosimeter, which is only useful at

room temperature. However, this change in sensitivity prompted us to re-evaluate whether we were still using the optimal concentrations of dosimetric components for HANor-HATet dosimeters.

### *3.3.2 Sulfuric Acid Optimization at Body Temperature*

To see if HANor-HATet was optimized at body temperature, the following concentrations of sulfuric acid were tested: 10 mM, 25 mM, 50 mM, and 100 mM. This study only focused on the change in optical absorbance from before irradiation to immediately after irradiation. Samples were irradiated at 0 Gy, 5 Gy, 10 Gy, 20 Gy, and 40 Gy.

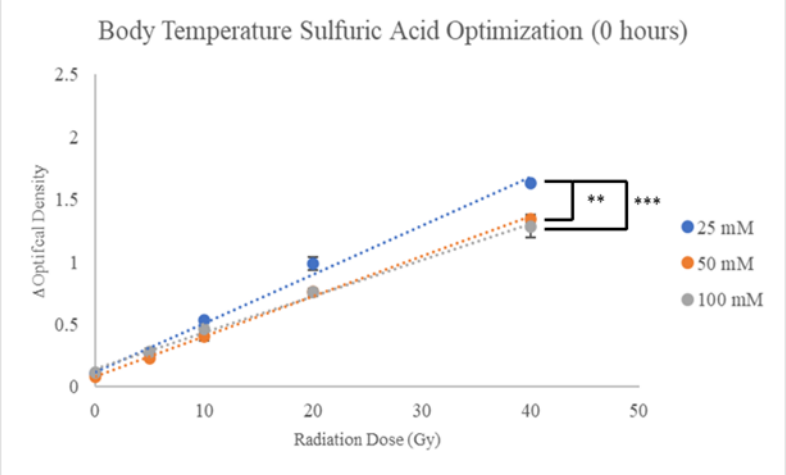


*Figure 13*. Sulfuric Acid Optimization at Body Temperature. Represents HANor-HATet samples containing 25 mM, 50 mM, and 100 mM sulfuric acid. All groups are kept at body temperature and scanned immediately after irradiation.

From the data, it appears that samples containing 25 mM seemed to follow a similar trend as in previous body temperature experiments. At 0 Gy, the 25 mM had no increase in optical density. On average, 25 mM samples irradiated with 5 Gy had a change in optical absorbance of just below 0.25 AU. The 25 mM samples irradiated with 10 Gy had an average gain in optical absorbance just under 0.5 AU. All 25 mM samples irradiated with 20 Gy had a gain of just short of 1 AU in optical density on average. Lastly, 25 mM samples irradiated with 40 Gy reached a change in optical absorbance of 1.6 AU just after irradiation. The 50 mM and 100 mM samples behaved the same, having overall less sensitivity to radiation than the 25 mM samples (Figure 13).

It seems that after 25 mM, increasing sulfuric acid concentration does not significantly increase sensitivity. In fact, it appears to hinder dosimetric sensitivity. For the comparison between 25 mM and 50 mM at 40 Gy, $p = 0.0017$. For the comparison between 25 mM and 100 mM at 40 Gy, $p = 0.0006$. From what is understood, it should be the case where increasing the concentration of sulfuric acid decreases the sensitivity of the dose response.[54] It should be noted that further characterization should be performed with MRI to verify the effects of increasing sulfuric acid.

### *3.3.3 Mohr's Salt Optimization at Body Temperature*

To further optimize the HANor-HATet dosimeter, a wider range of Mohr's Salt concentrations were tested. The concentrations tested are as follows: 0.1 mM, 0.5 mM, 0.75 mM, and 1 mM. This study only focused on the change in optical absorbance noted from before irradiation to immediately after irradiation. The dosages used to irradiate the samples are as follows: 0 Gy, 5 Gy, 10 Gy, 20 Gy, and 40 Gy.

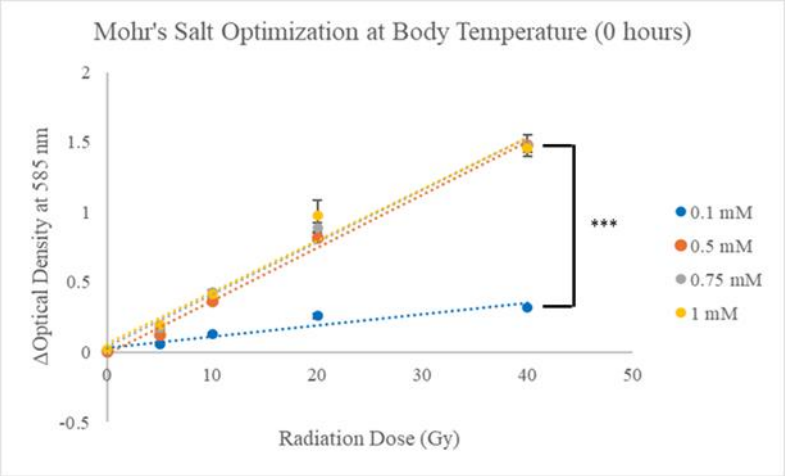


*Figure 14*. Mohr's Salt Optimization at Body Temperature. Represents HANor-HATet samples containing 0.1 mM, 0.5 mM, 0.75 mM, and 1 mM Mohr's salt. All groups are kept at body temperature.

At body temperature, the 0.1 mM samples follow a similar trend in optical absorbance gains compared to the room temperature results. Samples containing 0.5 mM seem to have almost identical sensitivities to radiation. At 0, 5, 10, 20, and 40 Gy, the approximate change in optical absorbance respectively measures as follows: 0, 0.2, 0.35, 0.7, and 1.4 AU. The only outlier is at 20 Gy where the sample groups seem to have slightly different gains in optical density. Other than this, their sensitivity curve to radiation remains uniformly the same for every dose the hydrogel was given (Figure 14).

Overall, it seems that lowering the Mohr's salt concentration does not impact sensitivity to radiation as long as it's not lowered past a certain threshold.[67] However, this needs further testing via MRI verification. In most cases, our hydrogels cannot gain optical density over 1.8 AU. This is due to Xylenol Orange being needed for optical

verification. Studies indicate that Xylenol Orange can only be used with a maximum concentration of 0.2 mM. After this, dosimeter hydrogels will start losing sensitivity to radiation.[61] The literature does not clarify why this happens, however, the fact remains that using 0.2 mM Xylenol Orange is a limiting factor when 1 mM of Mohr's salt is present. However, hydrogel verification through MRI does not have this limitation as Xylenol Orange is not a necessary component for this dose verification process.[46,63,64] It is therefore possible that the HANor-HATet dosimeters have a higher sensitivity peak than what is observed here with the optical data, which will need to be evaluated via MRI characterization of our hydrogel.

### *3.3.4 HANor-HATet Hydrogel Dosimeter Biocompatibility*

A culture of 10,000 cells were used to test the viability of the HANor-HATet dosimeter. Cultures were seeded in 24-well plates and exposed 100 µL cylindrical HANor-HATet dosimeter hydrogels using Transwell plates. Utilizing a plate reader, fluorescence was used to determine a standard curve that could be used to estimate the number of cells present in the culture based on metabolic activity. Fluorescence is read at an excitation wavelength of 570 nm and emission wavelength of 610 nm. AlamarBlue is used as an agent to determine the metabolic activity of the culture in this experiment. Sulfuric acid and Xylenol Orange were modulated in separate test groups. The sulfuric acid groups utilized in this study were as follows: 25 mM, 50 mM, and 100 mM. These groups used concentrations of 1 mM Mohr's Salt and 0.2 mM Xylenol Orange. The Xylenol Orange groups utilized in this study were as follows: 0.05 mM, 0.2 mM, and 0.5 mM. These groups used concentrations of 1 mM Mohr's Salt and 25 mM Sulfuric Acid. A blank gel group containing no dosimeter components, and a group not exposed to any

HANor-HATet hydrogels were utilized as controls. All groups utilized a sample size of n=3. When the fluorescence of the samples was measured, the supernatant of each well was taken and distributed into 3 wells of a 96-well plate, giving a total sample size of n=9 when the fluorescence of each sample group was measured. All samples were read after 1, 3, and 7 days in culture.

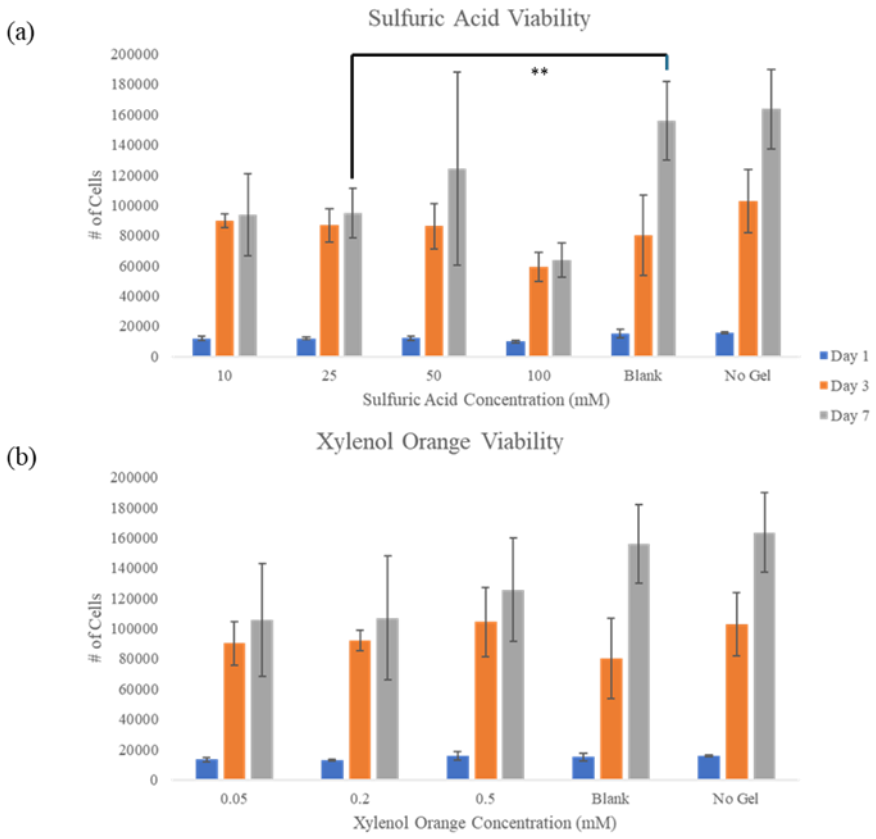


*Figure 15*. Cell Viability Assay. (a) Number of cells recorded on days 1, 3, and 7 for sulfuric acid groups. (b) Number of cells recorded on days 1, 3, and 7 for Xylenol Orange groups.

The control groups present a metric comparison for all other test groups. For the "Blank Gel" group, the number of cells grew to approximately 15,029 cells on day 1, 80,172 cells on day 3, and 155,747 cells on day 7. For the "No Gel" group, the number of cells grew to approximately 15,603 cells on day 1, 102,586 cells on day 3, and 163,506 cells on day 7.

For the sulfuric acid groups, the 10 mM, 25 mM, and 50 mM samples showed great promise of viability. The 10 mM sample culture grew to approximately 11,867 cells on day 1, 89,655 cells on day 3, and 93,678 cells on day 7. The 25 mM sample culture grew to approximately 11,867 cells on day 1, 86,782 cells on day 3, and 94,828 cells on day 7. The 50 mM sample culture grew to 11,983 cells on day 1, 86,207 cells on day 3, and 124,128 cells on day 7. The 100 mM sample culture grew to 9,856 cells on day 1, 59,195 cells on day 3, and 63,793 cells on day 7 (Figure 15a).

Every group of the xylenol orange modulated samples demonstrated great viability. The 0.05 mM sample culture grew to approximately 13,305 cells on day 1, 90,230 cells on day 3, and 105,747 cells on day 7. The 0.2 mM sample culture grew to approximately 12,931 cells on day 1, 91,954 cells on day 3, and 106,897 cells on day 7. The 0.5 mM sample culture grew to approximately 15,718 cells on day 1, 104,310 cells on day 3, and 125,575 cells on day 7 (Figure 15b).

There is a small difference between the control groups and the 10-50 mM sulfuric acid groups in terms of the number of cells in the culture on day 7. It should be noted that the p-value when comparing the group containing 25 mM of sulfuric acid, our optimal concentration, and the blank gel group is 0.0039, indicating a significant difference between the two groups. However, significant cell growth is observed in all sulfuric acid

groups. Even with the 100 mM sulfuric acid group, there is still a significant amount of cell growth within the culture by day 7. Although, due to the reduced number of cells by day 7, we wouldn't want to use 100 mM sulfuric acid during *in vivo* studies. This study also satisfies any concern that Xylenol Orange or Mohr's salt has any impact on cell viability. With this information, our team feels optimistic about taking the next steps in preparing for *in vivo* animal studies. In future studies, we plan to test our hydrogel's viability further through subcutaneous injections. Viability will be determined based off local inflammation and systemic cytotoxicity. It should be noted that no current animal studies utilizing an injectable dosimeter hydrogel exist as of now.

To investigate how the presence of sulfuric acid within our HANor-HATet dosimeter hydrogels affects local acidity, we conducted a pH test of the hydrogels over the course of 7 days. The hydrogels consisted of samples containing 0.2 mM Xylenol Orange, 1 mM Mohr's salt, and four different concentrations of sulfuric acid: 0 mM, 25 mM, 50 mM, and 100 mM. Hydrogels were made at quantities of 100 µL and topped with 1.5 mL of MilliQ water. The experiment was conducted with pH strips.

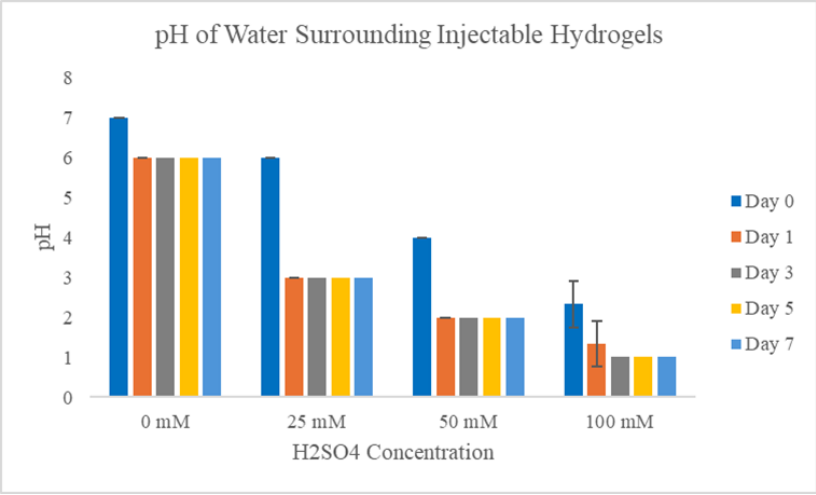

*Figure 16*. Evaluating HANor-HATet Hydrogel Dosimeter pH Over Time. HANor-HATet hydrogels containing 0.2 mM Xylenol Orange, 1 mM Mohr's salt, and varying concentrations of sulfuric acid: 0 mM, 25 mM, 50 mM, and 100 mM. The pH of the samples was measured over the course of 7 days using simple pH strips.

The 0 mM group started at a neutral pH of 7, dropped to 6, staying at this level for the duration of the experiment. The 25 mM group started at a slightly acidic pH of 6, dropping to 3 and remaining at that level for the next 6 days. The 50 mM group started at an acidic pH of 4, dropped to 2 by the next day, and remained in such a state for the entirety of the experiment. The 100 mM samples, on average, started at a very acidic pH of 2.33, dropping to an average of 1.33 the next day, then dropping to a highly acidic pH of 1 for rest of the study (Figure 16).

Overall, the results of this study were not exactly desirable. Most samples, other than the control group with a sulfuric acid concentration of 0 mM, had a pH of 3 or below following the initial day that the hydrogels were formed and submerged in MilliQ water. This is not ideal for us as at best, that's equivalent to the pH of lemon juice. At worst our pH reached a level of 1, which is equivalent to stomach acid. However, this is not entirely discouraging due to the conditions that the study had to be run under. As a basic principle, the components within the dosimeter hydrogels will diffuse out of the gel when submerged in water (Figure 17). This happens due to the principle of diffusion, where the concentration of a solute within a solution will distribute itself evenly within said solution. This general idea applies to hydrogels, which are 98% water, when they are submerged within MilliQ water. Due to the length of the pH strips, we had to submerge

the hydrogels in 1.5 mL of MilliQ water to ensure that the strips were able to take proper pH measurements. Due to material constraints, we could not just increase the amount of hydrogel used either. Therefore, the ratio of hydrogel to MilliQ water is 1:15. That being stated, instead of a slow and gradual diffusion that might happen in an *in vivo* environment with a lower ratio of hydrogel to water, a rapid expulsion of all Fricke components occurred to equally distribute the solutes, making the pH of the surrounding water much more acidic than it should be initially. If the ratio was lower, we speculate that the pH of the surrounding water would overall be less acidic. Furthermore, we are still not very concerned by these findings due to the results of the cell viability assay discussed previously.

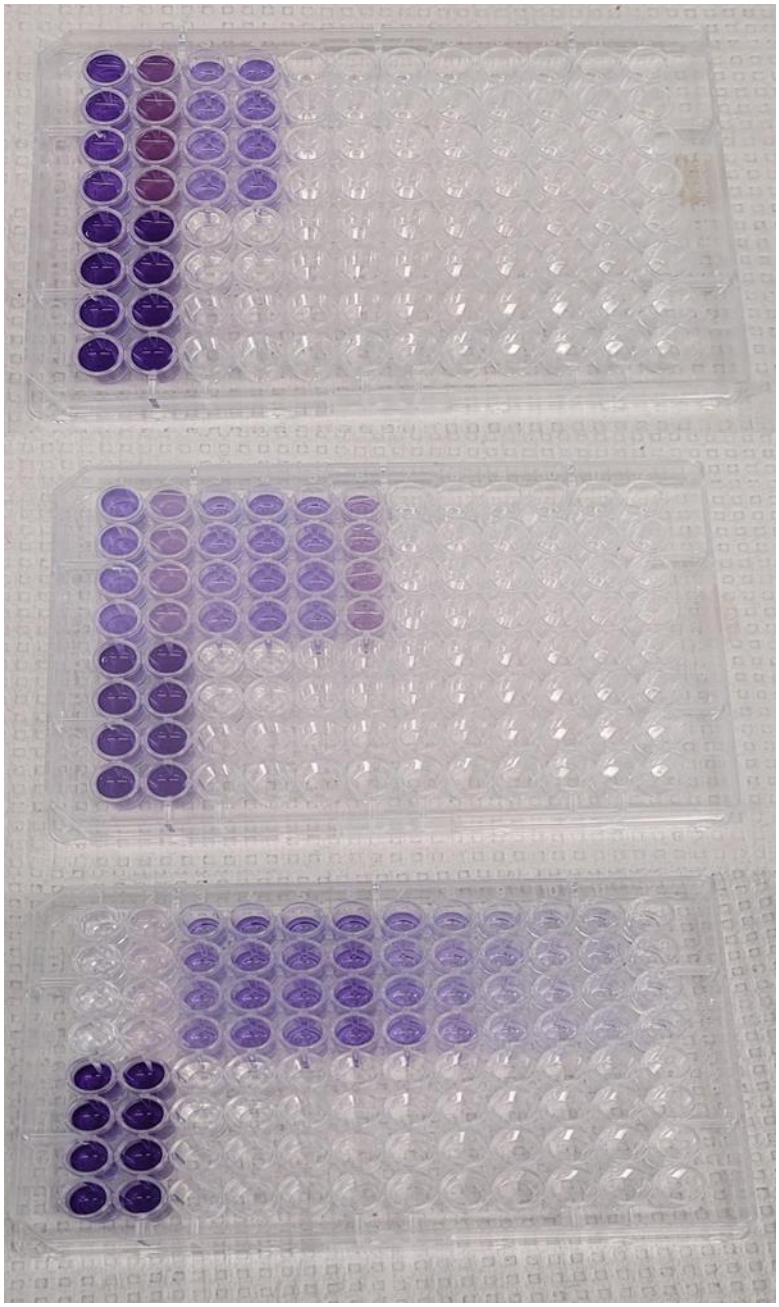

*Figure 17*. Diffusion of Fricke Components Out of Irradiated Hydrogels. Demonstrates the impact of diffusion on irradiated dosimeter hydrogels. The top half of the plate consists of hydrogels that had water taken out of the hydrogel wells (columns 1 & 2) and placed into the wells on the right (columns 3 & 4, 5 & 6, etc.). This process was done

every 2 days until the hydrogel wells lost all color. The bottom half of the plate consists of hydrogels that didn't have their water replaced (columns 1 & 2) and wells containing only MilliQ water (columns 3-12).

The results of the dosimeter hydrogels being placed in water without any solutes were observed in a prior study (Figure 17). In this study, we used hydrogels that were placed in two groups: one that had its water changed every few days, and one that didn't have its water changed at all. As demonstrated, the hydrogels that had their water changed every few days completely lost all color by the end of the study, indicating that all Fricke components had diffused out of the hydrogel (1 week). The hydrogels that didn't have their water changed retained their original color and optical density as Fricke components stopped diffusing out of the hydrogels due to equilibrium being reached. Ultimately, this shows that if the ratio of hydrogel to water is more even, then the entirety of the sulfuric acid component will not leak out into the surrounding liquid, lowering the pH of said liquid.

### *3.3.5 Radiation Patterning and Ferric Ion Diffusion*

One of the most important functions of a dosimeter hydrogel is to be able to accurately represent how much radiation a certain area is receiving. To this end, we formed dosimeter hydrogels in 100 mm cell culture dishes and utilized a LINAC to etch our lab's Vega Lab "VL" logo. Hydrogels were formed at 2% w/v and utilized 0.2 mM XO, 25 mM sulfuric acid, and 1 mM Mohr's Salt. In this sense, we compare the logo

results of the Gelatin dosimeter to the HANor-HATet dosimeter at room temperature. Logo results for the HANor-HATet at body temperature are also shown.

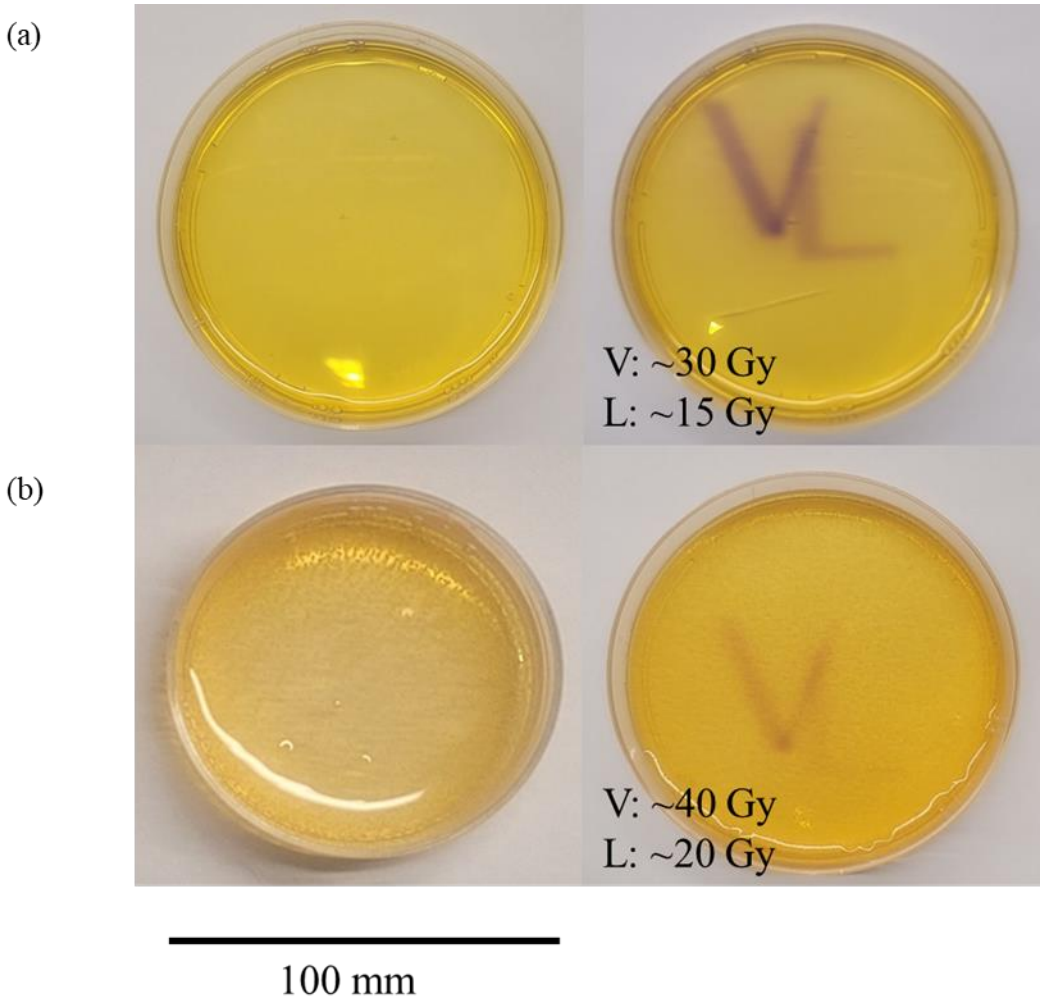


*Figure 18*. Spatial Radiation Pattern Analysis. A test performed to examine the ability of a dosimeter hydrogel to represent the radiation it is given spatially. To demonstrate this, our lab logo "VL" is etched into hydrogels. (a) A "before" and "after" snapshot of the gelatin dosimeter receiving patterned radiation. The "V" is given 30 Gy and the "L" is

given 15 Gy. (b) A “before” and “after” snapshot of the HANor-HATet dosimeter receiving patterned radiation. The “V” is given 40 Gy and the “L” is given 20 Gy.

The Gelatin dosimeter shows great spatiotemporal ability in the mapping of radiation doses. The “V” and “L” were formed into the Gelatin using 30 Gy and 15 Gy respectively. It is clearly demonstrated that the Gelatin holds the shape of our lab’s logo very well, having sharp, well-defined edges (Figure 18a). The HANor-HATet dosimeter shows relatively good spatiotemporal ability in the mapping of radiation doses. However, it should be noted that the Gelatin dosimeter provided a much clearer and sharper image at room temperature in comparison. The “V” and “L” were formed into the HANor-HATet using 40 Gy and 20 Gy respectively. Despite receiving a higher dosage, the logo isn’t quite as dark in color or refined in shape as it is for the Gelatin dosimeter. (Figure 18b).

Overall, it’s not surprising that the gelatin dosimeter ended up holding the shape of the logo better than the HANor-HATet dosimeter. As previously mentioned, the gelatin appeared to be more sensitive than the HANor-HATet dosimeter possibly due to the nitrogen bubbles present in the latter.[61] However, it is worth mentioning that we hypothesize the HANor-HATet irradiated at body temperature will perform significantly better than the samples irradiated at room temperature, leading to a better logo resolution. This is largely due to our earlier results with HANor-HATet irradiated at body temperature.

One major issue with dosimeter hydrogels is the quick rate of diffusion of $Fe^{3+}$ ions, often leading to the destruction of spatial radiation information.[68,71,72,74,83] For this

reason, we conducted a time trial after the previously discussed radiation patterning experiment to determine how prevalent the issue is in HANor-HATet. The trial lasted for approximately 24 hours after the samples were initially irradiated.

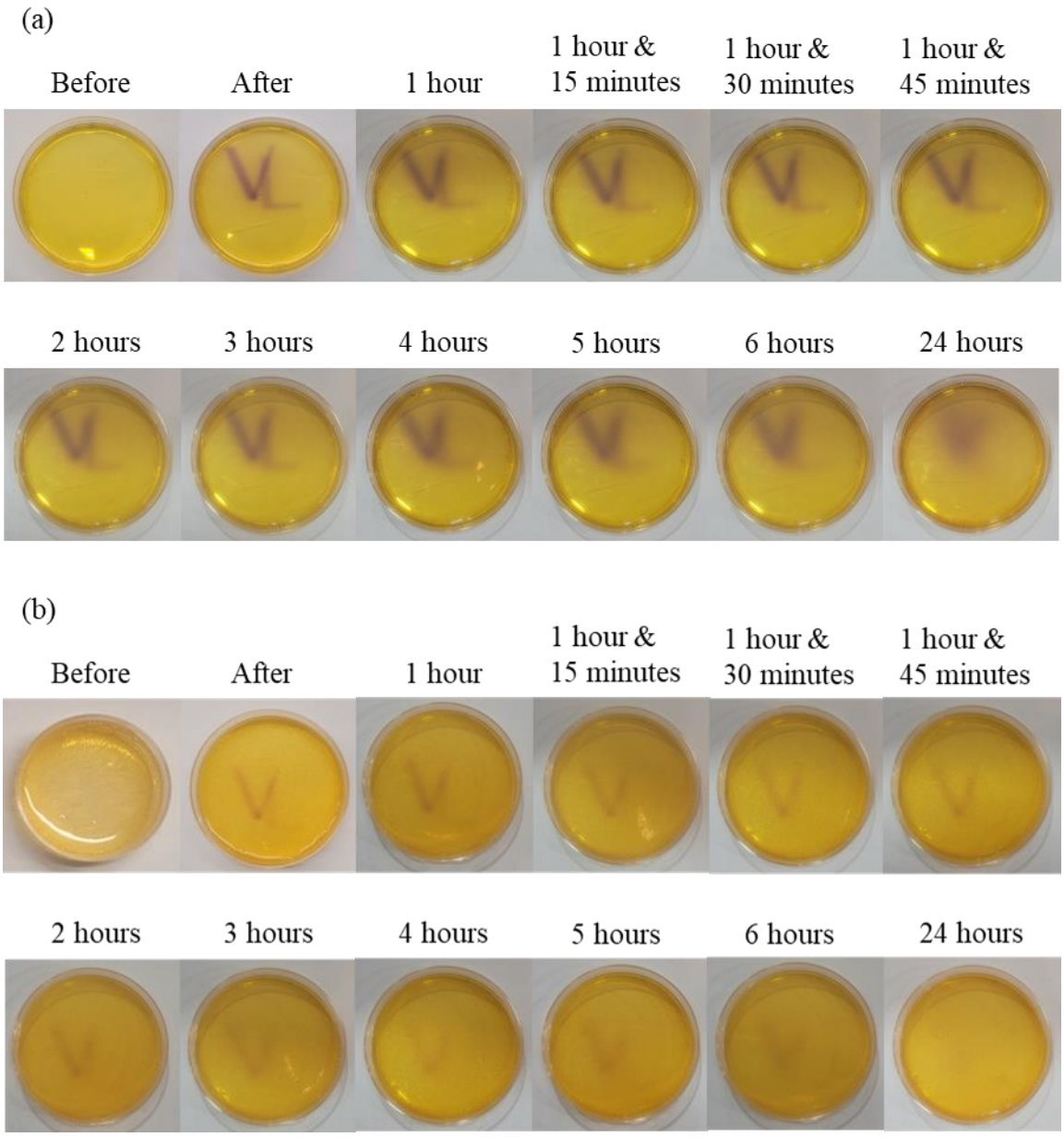

*Figure 19*. $Fe^{3+}$ Diffusion Time Trial. (a) The gelatin Fricke hydrogel from the spatial radiation patterning experiment observed over the course of 24 hours. (b) The HANor-HATet hydrogel from the spatial radiation patterning experiment observed over the course of 24 hours.

The data demonstrates a quick loss of spatial information over the course of the 24 hours. The irradiated area of the gelatin becomes noticeably more unclear in resolution just 1 hour after irradiation. After 2 hours it becomes increasingly uncanny from its original "VL" image until it becomes an unrecognizable purple blob by 24 after irradiation (Figure 19a). The HANor-HATet's resolution suffers more so than the gelatin. It does start to "blur" just 1 hour after irradiation, however, it also begins to lose its purple color, making the irradiated area become more undistinguishable from the surrounding unirradiated hydrogel. From 2 hours after irradiation and onwards, the image etched into the hydrogel becomes blurrier and loses its purple color until it almost disappears 24 hours post irradiation (Figure 19b).

Unfortunately, it becomes clear that the quick diffusion of $Fe^{3+}$ ions after irradiation remains an issue for the development of dosimeter hydrogels. However, this issue can be circumvented providing that the hydrogels are scanned as quickly as possible following irradiation. This should be made even more possible considering recent advances in technology. There have been recent developments in radiation therapy that allowed the creation of a magnetic resonance imaging LINAC system. Previously impossible with existing technology, it is now possible to take MRIs and irradiate a patient on the same machine. This system would theoretically allow for a radiation

treatment plan to be delivered and then immediately verified via MRI providing that a functional dosimeter hydrogel could be successfully injected to the site of treatment.[84]

### 3.4 Conclusions

In this study we aimed to evaluate the change in optical density as a function of radiation therapy at body temperature and further optimize dosimeter components of the HANor-HATet hydrogel at such conditions. Ultimately, it was discovered that not only will HANor-HATet function at body temperature, but it will also be overall more sensitive to radiation than it is at room temperature. It was also discovered that the optimal concentrations of dosimeter components used for the HANor-HATet dosimeter at room temperature are still optimal at body temperature: 0.2 mM Xylenol Orange, 25 mM sulfuric acid, and 1 mM Mohr's salt.

# Chapter 4

# Summary and Future Directions

## 4.1 Research Summary

We presented a thorough characterization of the HANor-HATet dosimeter hydrogel using spectrophotometric methods. It was determined that 0.2 mM Xylenol Orange is optimal for the HANor-HATet dosimeter. It was found that at a minimum, HANor-HATet dosimeters need a sulfuric acid concentration of 25 mM to properly function. Moreover, this same concentration is optimal for dosimetry in HANor-HATet hydrogels. It was discovered that Mohr's salt must be at a concentration of at least 0.5 mM for HANor-HATet to be functional as a dosimeter. The optimal concentration of Mohr's salt was found to be 1 mM. When compared to the gelatin dosimeter, we found that the HANor-HATet's sensitivity is slightly lower. However, it displays a strong, distinct, and linear dose response, much like gelatin dosimeters. Spectral analysis also displayed that our hydrogel is not only functional at body temperature, but also more sensitive to radiation than it is at room temperature. The optimal concentrations for dosimeter components in HANor-HATet dosimeters at room temperature remain the optimal concentrations for HANor-HATet dosimeters at body temperature.

## 4.2 Future Directions

I was able to complete the most crucial aspects of the hydrogel study in my time here, including a thorough optical characterization of the HANor-HATet dosimeter, a comparison of the HANor-HATet dosimeter to the gelatin Fricke, and a biocompatibility study. However, there are other crucial studies that must be done in the future to enable a pathway to clinical trials, which are summarized in the next sections.

### *4.2.1 HANor-HATet MRI Characterization*

One major study that should be conducted is the characterization of the HANor-HATet dosimeter using MRI. We have discovered many properties of our dosimeter hydrogel through optical studies, however, any *in-vivo* testing will need to scan the hydrogels using MRI. It must be confirmed that the linear dose response of the hydrogels we saw during optical testing carries over in principle to MRI testing. Moreover, it might make an interesting study to test the maximum sensitivity and longevity of the HANor-HATet once the primary inhibitor on longevity, the Xylenol Orange, is no longer needed to scan the hydrogels. Most importantly, characterizing our hydrogel with MRI will allow us to scan a three-dimensional snapshot of the radiation that it has absorbed.

### *4.2.2 Rodent Tumor Models: Dosage Verification Utilizing HANor-HATet Dosimeters*

Following a complete characterization of the HANor-HATet hydrogels via MRI, animal studies should be the next immediate goal. After basic viability is tested through the subcutaneous injections of our injectable dosimeter hydrogels in deceased mice, a basic radiation experiment should follow. Injecting our hydrogel into deceased mice following the creation of a radiation treatment plan, the mice should be irradiated to certain dosages at a chosen target site, followed by dosage verification via MRI.

## 4.3 Concluding Remarks

In this thesis, an injectable radiation dosimeter that can function at body temperature was developed using HANor-HATet as base matrix for dosimeter components. Through the optimization of these components, HANor-HATet proved to be a strong dosimeter that compares well to gelatin dosimeters, the previous gold standard of hydrogel dosimetry. This dosimeter was able to work at body temperature and gained

optical density as a function of radiation. This is a pivotal step as no dosimeter hydrogel has ever functioned at body temperature. Hopefully, this can potentially lead to an injectable hydrogel dosimeter that can be used clinically to validate the dosage of radiation that cancer radiation therapy patients receive in the treatment of hard tumors.

## References


1. Organization, W. H. Global cancer burden growing, amidst mounting need for services. *2024-02-01)[2024-02-25]. https://www. who. int/news/item/01-02-2024-global-cancer-burden-growing--amidst-mountingneed-for-services* Preprint at (2024).
2. Types of Cancer Treatment - NCI. https://www.cancer.gov/about-cancer/treatment/types.
3. Blood Cancer Therapy and Treatment | UPMC Hillman Cancer Center. https://hillman.upmc.com/cancer-care/blood/treatment.
4. Hormone therapy | Canadian Cancer Society. https://cancer.ca/en/treatments/treatment-types/hormone-therapy.
5. Treatment For Cancer | Cancer Treatment Options | American Cancer Society. https://www.cancer.org/cancer/managing-cancer/treatment-types.html.
6. Radiation therapy - Mayo Clinic. https://www.mayoclinic.org/tests-procedures/radiation-therapy/about/pac-20385162.
7. Chemotherapy - Mayo Clinic. https://www.mayoclinic.org/tests-procedures/chemotherapy/about/pac-20385033.
8. Chemotherapy - NHS. https://www.nhs.uk/conditions/chemotherapy/.
9. Chemotherapy - Mayo Clinic. https://www.mayoclinic.org/tests-procedures/chemotherapy/about/pac-20385033.
10. Surgical Procedures for Basal & Squamous Cell Skin Cancers | NYU Langone Health. https://nyulangone.org/conditions/basal-squamous-cell-skin-cancers/treatments/surgical-procedures-for-basal-squamous-cell-skin-cancers.
11. Types of surgery for soft tissue sarcoma | Soft tissue sarcoma | Cancer research UK. https://www.cancerresearchuk.org/about-cancer/soft-tissue-sarcoma/treatment/surgery/types.
12. Surgery to remove melanoma skin cancer | Cancer Research UK. https://www.cancerresearchuk.org/about-cancer/melanoma/treatment/surgery/surgery-remove-melanoma.
13. How Surgery Is Used for Cancer | Curative Surgery | American Cancer Society. https://www.cancer.org/cancer/managing-cancer/treatment-types/surgery/how-surgery-is-used-for-cancer.html.
14. Sequence of Treatment. https://www.breastcancer.org/treatment/planning/sequence-of-treatment.

15. Definition of curative surgery - NCI Dictionary of Cancer Terms - NCI. https://www.cancer.gov/publications/dictionaries/cancer-terms/def/curative-surgery.

16. Surgery for Cancer - NCI. https://www.cancer.gov/about-cancer/treatment/types/surgery.

17. What is cancer surgery? | Cancer Research UK. https://www.cancerresearchuk.org/about-cancer/treatment/surgery/about.

18. Hormone therapy for cancer | Cancer Research UK. https://www.cancerresearchuk.org/about-cancer/treatment/hormone-therapy/for-cancer.

19. Hormone Therapy for Cancer - NCI. https://www.cancer.gov/about-cancer/treatment/types/hormone-therapy.

20. Hormone therapy for prostate cancer - Mayo Clinic. https://www.mayoclinic.org/tests-procedures/hormone-therapy-for-prostate-cancer/about/pac-20384737.

21. Hormone therapy for breast cancer - Mayo Clinic. https://www.mayoclinic.org/tests-procedures/hormone-therapy-for-breast-cancer/about/pac-20384943.

22. Hormone Therapy for Cancer - NCI. https://www.cancer.gov/about-cancer/treatment/types/hormone-therapy.

23. Dobosz, P. & Dzieciątkowski, T. The Intriguing History of Cancer Immunotherapy. *Front Immunol* **10**, 2965 (2019).

24. CAR T Cell Therapy | Penn Medicine. https://www.pennmedicine.org/cancer/navigating-cancer-care/treatment-types/immunotherapy/what-is-car-t-therapy.

25. Stanford Medicine delivers first FDA-approved cell-based therapy for solid tumors | News Center | Stanford Medicine. https://med.stanford.edu/news/all-news/2024/05/car-t-melanoma.html.

26. Immunotherapy By Cancer Type | Cancer Research Institute. https://www.cancerresearch.org/immunotherapy-by-cancer-type.

27. Immunotherapy for Cancer - NCI. https://www.cancer.gov/about-cancer/treatment/types/immunotherapy.

28. CAR T-Cell Therapy: How to Manage Costs and Get Financial Assistance. https://www.webmd.com/cancer/lymphoma/features/navigate-finances-car-t-cell-therapy.

29. Disease Control Priorities, Third Edition (Volume 3): Cancer - Google Books. https://books.google.com/books?hl=en&lr=&id=Ulz1CgAAQBAJ&oi=fnd&pg=PP1&dq=17.%09Gelband,+H.,+Jha,+P.,+Sankaranarayanan,+R.,+%26+Horton,+S.+(2015).+Disease+Control+Priorities,+Third+Edition+(Volume+3):+Cancer.+World+Bank+Publications.&ots=P_MJklHpXW&sig=B6Ej_HTBFYZ28Uv-FgrhBV5aA4o#v=onepage&q=17.%09Gelband%2C%20H.%2C%20Jha%2C%20P.%2C%20Sankaranarayanan%2C%20R.%2C%20%26%20Horton%2C%20S.%20(2015).%20Disease%20Control%20Priorities%2C%20Third%20Edition%20(Volume%203)%3A%20Cancer.%20World%20Bank%20Publications.&f=false.

30. Radiation therapy - Mayo Clinic. https://www.mayoclinic.org/tests-procedures/radiation-therapy/about/pac-20385162.

31. Radiation therapy for Lung Cancer | Cancer Council NSW. https://www.cancercouncil.com.au/lung-cancer/treatment/radiotherapy/.

32. Radiation Therapy for Cancer - NCI. https://www.cancer.gov/about-cancer/treatment/types/radiation-therapy.

33. Boekhoff, M. *et al.* An in-silico assessment of the dosimetric benefits of MR-guided radiotherapy for esophageal cancer patients. *Radiotherapy and Oncology* **162**, 76–84 (2021).

34. Radiation Therapy Process | Stony Brook Cancer Center. https://cancer.stonybrookmedicine.edu/RadiationTherapyProcess.

35. About Your External Beam Radiation Therapy | Memorial Sloan Kettering Cancer Center. https://www.mskcc.org/cancer-care/patient-education/external-beam-radiation-therapy#section-3.

36. Image Guided Radiation Therapy & Radiotherapy | UPMC. https://hillman.upmc.com/cancer-care/radiation-oncology/treatment/external-beam/image-guided-radiotherapy-igrt.

37. Intensity modulated radiotherapy (IMRT) | Cancer treatment | Cancer Research UK. https://www.cancerresearchuk.org/about-cancer/treatment/radiotherapy/external/types/intensity-modulated-radiotherapy-imrt.

38. Image-Guided Radiation Therapy (IGRT). https://my.clevelandclinic.org/health/procedures/image-guided-radiation-therapy-igrt.

39. Radiotherapy of the brain (fractionated) | Mayfield Brain & Spine. https://mayfieldclinic.com/pe-radiotherapybrain.htm.

40. Fractionation and Radiation | OncoLink. https://www.oncolink.org/cancer-treatment/radiation/support/fractionation-and-radiation.

41. Gray (Gy) | NRC.gov. https://www.nrc.gov/reading-rm/basic-ref/glossary/gray-gy.html.

42. Radiation Therapy Dosage. https://www.news-medical.net/health/Radiation-Therapy-Dosage.aspx.

43. Facts About Radiation from Space (Cosmic Radiation) | Radiation and Your Health | CDC. https://www.cdc.gov/radiation-health/data-research/facts-stats/cosmic-radiation.html.

44. Radiation dosimetry: mSv & mGy. https://www.mun.ca/biology/scarr/Radiation_definitions.html.

45. Side Effects of Radiation Therapy | Radiation Effects on Body | American Cancer Society. https://www.cancer.org/cancer/managing-cancer/treatment-types/radiation/effects-on-different-parts-of-body.html.

46. Chen, Y. L. *et al.* Dose verification of a clinical intensity-modulated radiation therapy eye case by the magnetic resonance imaging of N-isopropylacrylamide gel dosimeters. *Radiation Physics and Chemistry* **104**, 188–191 (2014).

47. Kraan, A. C. Range verification methods in particle therapy: Underlying physics and Monte Carlo modelling. *Front Oncol* **5**, 139363 (2015).

48. Dosimeter Definition & Meaning - Merriam-Webster. https://www.merriam-webster.com/dictionary/dosimeter.

49. Radiation Dosimeters | Homeland Security. https://www.dhs.gov/publication/radiation-dosimeters.

50. Common Dosimeters | Oncology Medical Physics. https://oncologymedicalphysics.com/common-dosimeters/.

51. Parwaie, W., Refahi, S., Ardekani, M. A. & Farhood, B. Different Dosimeters/Detectors Used in Small-Field Dosimetry: Pros and Cons. *J Med Signals Sens* **8**, 195 (2018).

52. Geiger Counters: Measuring Radiation Through Clicking Sounds. https://www.popularmechanics.com/science/a42221680/how-do-geiger-counters-measure-radiation/.

53. Casolaro, P. *et al.* Real-time dosimetry with radiochromic films. *Scientific Reports 2019 9:1* **9**, 1–11 (2019).

54. Gallo, S. *et al.* Does the gelation temperature or the sulfuric acid concentration influence the dosimetric properties of radiochromic PVA-GTA Xylenol Orange Fricke gels? *Radiation Physics and Chemistry* **160**, 35–40 (2019).

55. Locarno, S. & De Deene, Y. Radiation Dosimetry by Use of Radiosensitive Hydrogels and Polymers: Mechanisms, State-of-the-Art and Perspective from 3D to 4D. *Gels 2022, Vol. 8, Page 599* **8**, 599 (2022).

56. Marrale, M. & D'errico, F. Hydrogels for Three-Dimensional Ionizing-Radiation Dosimetry. *Gels 2021, Vol. 7, Page 74* **7**, 74 (2021).

57. Macchione, M. A., Lechón Páez, S., Strumia, M. C., Valente, M. & Mattea, F. Chemical Overview of Gel Dosimetry Systems: A Comprehensive Review. *Gels* **8**, (2022).

58. Alves, A. V. S. *et al.* Investigation of chelating agents/ligands for Fricke gel dosimeters. *Radiation Physics and Chemistry* **150**, 151–156 (2018).

59. Collura, G. *et al.* Analysis of the response of PVA-GTA Fricke-gel dosimeters with clinical magnetic resonance imaging. *Nucl Instrum Methods Phys Res B* **414**, 146–153 (2018).

60. Colnot, J., Huet, C., Gschwind, R. & Clairand, I. Characterisation of two new radiochromic gel dosimeters TruView$^{TM}$ and ClearView$^{TM}$ in combination with the vista$^{TM}$ optical CT scanner: A feasibility study. *Physica Medica* **52**, 154–164 (2018).

61. Davies, J. B. & Baldock, C. Sensitivity and stability of the Fricke–gelatin–xylenol orange gel dosimeter. *Radiation Physics and Chemistry* **77**, 690–696 (2008).

62. De Deene, Y. Gel-based Radiation Dosimetry Using Quantitative MRI. *New Developments in NMR* **2020-January**, 275–357 (2020).

63. Konradsson, E. *et al.* Polymer gel dosimetry for experimental verification of conformal small animal irradiation at a preclinical research platform. *J Phys Conf Ser* **2630**, 012034 (2023).

64. Liosi, G. M. *et al.* Fricke-gel dosimeter: overview of Xylenol Orange chemical behavior. *Radiation Physics and Chemistry* **140**, 74–77 (2017).

65. Maeyama, T., Fukunishi, N., Ishikawa, K. L., Fukasaku, K. & Fukuda, S. Organic-Gelatin-Free Nanocomposite Fricke Gel Dosimeter. *Journal of Physical Chemistry B* **121**, 4238–4246 (2017).

66. Piotrowski, M., Maras, P., Wach, R., Kadlubowski, S. & Kozicki, M. Impact of Salt on Thermal Stability and Dose Response of the Fricke-XO-Pluronic F-127 3D Radiotherapy Dosimeter. *Materials* **15**, (2022).

67. Scotti, M. *et al.* How Xylenol Orange and Ferrous Ammonium Sulphate Influence the Dosimetric Properties of PVA–GTA Fricke Gel Dosimeters: A Spectrophotometric Study. *Gels 2022, Vol. 8, Page 204* **8**, 204 (2022).

68. Schreiner, L. J. Review of Fricke gel dosimeters. *J Phys Conf Ser* **3**, 9 (2004).

69. Soliman, Y. S., El Gohary, M. I., Abdel Gawad, M. H., Amin, E. A. & Desouky, O. S. Fricke gel dosimeter as a tool in quality assurance of the radiotherapy treatment plans. *Applied Radiation and Isotopes* **120**, 126–132 (2017).

70. Vaiente, M. *et al.* Fricke gel dosimeter with improved sensitivity for low-dose-level measurements. *J Appl Clin Med Phys* **17**, 402–417 (2016).

71. Marini, A. *et al.* Fricke gel dosimeters with low-diffusion and high-sensitivity based on a chemically cross-linked PVA matrix. *Radiat Meas* **106**, 618–621 (2017).

72. Maeyama, T. *et al.* A diffusion-free and linear-energy-transfer-independent nanocomposite Fricke gel dosimeter. *Radiation Physics and Chemistry* **96**, 92–96 (2014).

73. Pang, Z., Deeth, H., Sopade, P., Sharma, R. & Bansal, N. Rheology, texture and microstructure of gelatin gels with and without milk proteins. *Food Hydrocoll* **35**, 484–493 (2014).

74. Pedersen, T. V., Olsen, D. R. & Skretting, A. Measurement of the ferric diffusion coefficient in agarose and gelatine gels by utilization of the evolution of a radiation induced edge as reflected in relaxation rate images. *Phys Med Biol* **42**, 1575 (1997).

75. Liu, M. *et al.* Injectable hydrogels for cartilage and bone tissue engineering. *Bone Research 2017 5:1* **5**, 1–20 (2017).

76. Overstreet, D. J., Dutta, D., Stabenfeldt, S. E. & Vernon, B. L. Injectable hydrogels. *J Polym Sci B Polym Phys* **50**, 881–903 (2012).

77. Yu, L. & Ding, J. Injectable hydrogels as unique biomedical materials. *Chem Soc Rev* **37**, 1473–1481 (2008).

78. Desai, R. M., Koshy, S. T., Hilderbrand, S. A., Mooney, D. J. & Joshi, N. S. Versatile click alginate hydrogels crosslinked via tetrazine–norbornene chemistry. *Biomaterials* **50**, 30–37 (2015).

79. Gultian, K. A. *et al.* Injectable hydrogel with immobilized BMP-2 mimetic peptide for local bone regeneration. *Frontiers in Biomaterials Science* **1**, 948493 (2022).

80. Koshy, S. T. *et al.* Click-Crosslinked Injectable Gelatin Hydrogels. *Adv Healthc Mater* **5**, 541 (2016).

81. Kumar, P., Nagarajan, A. & Uchil, P. D. Analysis of Cell Viability by the alamarBlue Assay. *Cold Spring Harb Protoc* **2018**, pdb.prot095489 (2018).

82. Smith, I. W. M. The temperature-dependence of elementary reaction rates: beyond Arrhenius. *Chem Soc Rev* **37**, 812–826 (2008).

83. Olsson, L. E. Diffusion of ferric ions in agarose dosimeter gels. *Article in Physics in Medicine & Biology* (2000) doi:10.1088/0031-9155/37/12/006.

84. Lagendijk, J. J. W., Raaymakers, B. W. & van Vulpen, M. The Magnetic Resonance Imaging–Linac System. *Semin Radiat Oncol* **24**, 207–209 (2014).